



**HAL**  
open science

## **Drivers and CO<sub>2</sub> flux budgets in a Sahelian *Faidherbia albida* agro-silvo-pastoral parkland: Insights from continuous high-frequency soil chamber measurements and Eddy Covariance**

Seydina Mohamad Ba, Olivier Roupsard, Lydie Chapuis-Lardy, Frédéric Bouvery, Yélognissè Agbohessou, Maxime Duthoit, Aleksander Wieckowski, Torbern Tagesson, Mohamed Habibou Assouma, Espoir Koudjo Gaglo, et al.

### ► **To cite this version:**

Seydina Mohamad Ba, Olivier Roupsard, Lydie Chapuis-Lardy, Frédéric Bouvery, Yélognissè Agbohessou, et al.. Drivers and CO<sub>2</sub> flux budgets in a Sahelian *Faidherbia albida* agro-silvo-pastoral parkland: Insights from continuous high-frequency soil chamber measurements and Eddy Covariance. 2025. <hal-05387486>

**HAL Id: hal-05387486**

**<https://hal.science/hal-05387486v1>**

Preprint submitted on 5 Dec 2025

HAL is a multi-disciplinary open access archive for the deposit and dissemination of scientific research documents, whether they are published or not. The documents may come from teaching and research institutions in France or abroad, or from public or private research centers.

L'archive ouverte pluridisciplinaire HAL, est destinée au dépôt et à la diffusion de documents scientifiques de niveau recherche, publiés ou non, émanant des établissements d'enseignement et de recherche français ou étrangers, des laboratoires publics ou privés.



Distributed under a Creative Commons CC BY 4.0 - Attribution - International License



1 **Drivers and CO<sub>2</sub> flux budgets in a Sahelian *Faidherbia albida* agro-silvo-pastoral parkland:**  
2 **Insights from continuous high-frequency soil chamber measurements and Eddy**  
3 **Covariance.**

4 Seydina Mohamad Ba <sup>a d</sup>, Olivier Roupsard <sup>b c d</sup>, Lydie Chapuis-Lardy <sup>c f</sup>, Frédéric Bouvery <sup>g</sup>,  
5 Yélognissè Agbohessou <sup>c e</sup>, Maxime Duthoit <sup>c e</sup>, Aleksander Wieckowski <sup>h</sup>, Torbern Tagesson <sup>h</sup>,  
6 Mohamed Habibou Assouma <sup>i j k</sup>, Espoir K. Gaglo <sup>a d</sup>, Claire Delon <sup>l</sup>, Bienvenu Sambou <sup>a</sup>, Dominique  
7 Serça <sup>l</sup>

8 <sup>a</sup> Faculté des Sciences et Techniques (FST), Institut des Sciences de l'Environnement (ISE), Université  
9 Cheikh Anta Diop (UCAD) de Dakar, 5005, Dakar-Fann, Sénégal

10 <sup>b</sup> CIRAD, UMR Eco&Sols, Dakar, Sénégal

11 <sup>c</sup> Eco&Sols, Univ Montpellier, CIRAD, INRAE, Institut Agro, IRD, Montpellier, France

12 <sup>d</sup> LMI IESOL, Centre IRD-ISRA de Bel Air, Route des hydrocarbures, 18524, Dakar, Sénégal

13 <sup>e</sup> CIRAD, UMR Eco&Sols, Université de Montpellier, Cirad, INRAE, IRD, Institut Agro Montpellier, 2 place  
14 Viala, Montpellier, France

15 <sup>f</sup> IRD, UMR Eco&Sols, Université de Montpellier, Cirad, INRAE, IRD, Institut Agro Montpellier, 2 place Viala,  
16 Montpellier, France

17 <sup>g</sup> INRAE, 147 rue de l'Université, 75338 Paris, France

18 <sup>h</sup> Department of Physical Geography and Ecosystem Science, Lund University, Sölvegatan 12, S-223 62 Lund,  
19 Sweden

20 <sup>i</sup> CIRAD, UMR SELMET, dP ASAP, Bobo Dioulasso, Burkina Faso

21 <sup>j</sup> SELMET, CIRAD, INRAE, Univ Montpellier, Institut SupAgro, Montpellier, France

22 <sup>k</sup> Centre International de Recherche-Développement sur l'Élevage en zone Subhumide (CIRDES), N°559, rue  
23 5-31 Avenue du Gouverneur Louveau, Bobo-Dioulasso, Burkina Faso

24 <sup>l</sup> Laboratoire d'Aérodynamique, Université de Toulouse, CNRS, IRD, 14 Avenue Edouard Belin, 31400 Toulouse,  
25 France

26 **Corresponding authors:**

27 Seydina Mohamad Ba: [seydina.ba@ird.fr](mailto:seydina.ba@ird.fr)

28 Olivier Roupsard: [olivier.roupsard@cirad.fr](mailto:olivier.roupsard@cirad.fr)



29 **Highlights:**

- 30     • Long-term high frequency CO<sub>2</sub> flux measurements using automated static  
31       chambers in a Sahelian *F. albida* parkland.
- 32     • Empirical gap-filling and flux partitioning methods validated against Eddy  
33       Covariance GPP.
- 34     • Fluxes peaked during the rainy season in both FS and Sh, driven mainly by soil  
35       moisture and leaf area.
- 36     • *F. albida* trees enhance CO<sub>2</sub> fluxes under canopies ("fertile island" effect) and  
37       account for ~50% of annual ecosystem GPP.



38 **ABSTRACT:**

39 Agroforestry systems — combining trees with crops and/or livestock — are increasingly  
40 promoted as sustainable and climate-resilient land-use strategies. Despite their widespread  
41 presence in the Sahel, experimental data on their potential as carbon sinks are scarce. This study  
42 presents a full-year, high-frequency dataset of CO<sub>2</sub> fluxes in a Sahelian agro-silvo-pastoral  
43 parkland dominated by *F. albida*, located in Senegal's groundnut basin. CO<sub>2</sub> fluxes were  
44 continuously measured using automated static chambers, allowing the quantification of soil and  
45 crop respiration (R<sub>ch</sub>), gross primary production (GPP<sub>ch</sub>), and net carbon exchange (FCO<sub>2ch</sub>)  
46 under both full sun and shaded (under tree canopies) environments.

47 Seasonal patterns of CO<sub>2</sub> fluxes were similar in both environments, with peaks during the rainy  
48 season. R<sub>ch</sub> and GPP<sub>ch</sub> were significantly higher under tree canopies, indicating a 'fertile island'  
49 effect. CO<sub>2</sub> flux variability was primarily driven by soil moisture and leaf area index. Chamber-  
50 based GPP estimates closely matched those from Eddy Covariance measurements. On an annual  
51 scale, *F. albida* trees contributed approximately 50% of total ecosystem GPP, with a carbon use  
52 efficiency of 0.48. Net annual CO<sub>2</sub> exchange was estimated at  $-1.4 \pm 0.02$  and  $-1.8 \pm 0.01$  Mg C-  
53 CO<sub>2</sub> ha<sup>-1</sup> using chamber and Eddy Covariance methods, respectively. These findings underscore  
54 the role of *F. albida*-based agroforestry systems as effective carbon sinks in Sahelian landscapes,  
55 supporting their potential contribution to climate change mitigation.

56 **Keywords:** Sahelian agro-silvo-pastoral systems, CO<sub>2</sub> fluxes, automated static chambers, Eddy  
57 Covariance, 'fertile island effect' of trees, carbon budgets.



## 58 1. Introduction

59 Plant photosynthesis and respiration —both autotrophic (plant) and heterotrophic (microbial)—  
60 are fundamental processes driving carbon dioxide (CO<sub>2</sub>) fluxes in terrestrial ecosystems  
61 (Lambers et al., 2008; Raich et al., 2014; Reichle, 2020). Accurate quantification of these processes  
62 is critical for assessing ecosystem carbon (C) sink potential (Baldocchi, 2020), particularly for  
63 informing climate-smart land management strategies.

64 To capture these processes at the ecosystem scale, the Eddy Covariance (EC) technique has  
65 emerged as a transformative method, enabling continuous and high-frequency CO<sub>2</sub> flux  
66 measurements (Baldocchi, 2003, 2008). Extensive EC networks in Europe (Stojanović et al.,  
67 2024), Asia (Yu et al., 2011), and the Americas (Chu et al., 2021) have significantly advanced our  
68 understanding of the global C cycle. In contrast, sub-Saharan Africa remains critically  
69 underrepresented (Bombelli et al., 2009; Houghton & Hackler, 2006; Williams et al., 2007).  
70 Although some studies have used EC (Ardö et al., 2008; Brümmer et al., 2008; Merbold et al., 2009;  
71 Tagesson et al., 2016), static chambers (Assouma et al., 2017; Owusu et al., 2024; Rosenstock et  
72 al., 2016; Wachye et al., 2020), or modeling approaches (Agbohessou et al., 2023, 2024; Delon  
73 et al., 2019; Rahimi et al., 2021), they remain sparse and methodologically heterogeneous, limiting  
74 comparability and regional C budget integration.

75 Among these underrepresented landscapes, agroforestry systems in the Sahel— particularly  
76 agro-silvo-pastoral systems (ASPS) that combine trees, crops, and livestock— are increasingly  
77 promoted for sustainable land management and climate resilience (Cardinael et al., 2021; Gupta  
78 et al., 2023; Mbow et al., 2014; Stetter & Sauer, 2024). However, the structural and functional  
79 heterogeneity of these systems poses significant challenges for accurately quantifying and  
80 upscaling C fluxes. *Faidherbia albida*, a keystone agroforestry tree species in these ASPs (Leroux  
81 et al., 2022; Lu et al., 2022), is of particular interest due to its reverse phenology, capacity to  
82 enhance soil fertility and crop yields (Bayala et al., 2020; Roupsard et al., 2020; Sileshi et al., 2016;  
83 2020). Yet, its functional role in modulating both the magnitude and seasonal dynamics of CO<sub>2</sub>  
84 fluxes remains poorly understood.

85 Addressing this knowledge gap requires integrated approaches capable of capturing both  
86 aggregate and component-specific CO<sub>2</sub> fluxes. While EC remains the gold standard method for CO<sub>2</sub>  
87 flux measurements at the landscape scale (Baldocchi, 2003), it captures net ecosystem exchange  
88 (NEE) as an aggregate signal, without separating the contributions from individual compartments  
89 such as soil, crops, and trees. This limits its utility for disentangling processes and attributing  
90 sources in heterogeneous systems like ASPs. Automatic static chambers provide a valuable  
91 complement to EC, as they enable continuous, high-frequency measurements at finer scales and  
92 at the level of specific ecosystem components. This approach facilitates component-specific  
93 quantification of CO<sub>2</sub> fluxes, particularly from soil and crop compartments (Luo & Zhou, 2006;



94 Denmead, 2008; Zaman et al., 2021). When combined with EC, this dual-method approach  
95 strengthens source attribution and improves the upscaling of fluxes across complex agroforestry  
96 landscapes.

97 This study presents one of the first integrated quantification of CO<sub>2</sub> fluxes in a Sahelian ASPS  
98 dominated by *F. albida*, combining EC and automatic static chambers.

99 Specifically, we aim to (1) conduct year-round, high-frequency *in situ* CO<sub>2</sub> flux measurements  
100 from soil and crops using automated static chambers; (2) partition the net CO<sub>2</sub> fluxes (FCO<sub>2</sub>ch)  
101 into respiration (R<sub>ch</sub>) and photosynthesis (GPP<sub>ch</sub>); (3) investigate the environmental drivers of  
102 fluxes and the spatial variability linked to tree presence; and (4) compare chamber-based flux  
103 estimates with ecosystem-scale measurements derived from the EC method.



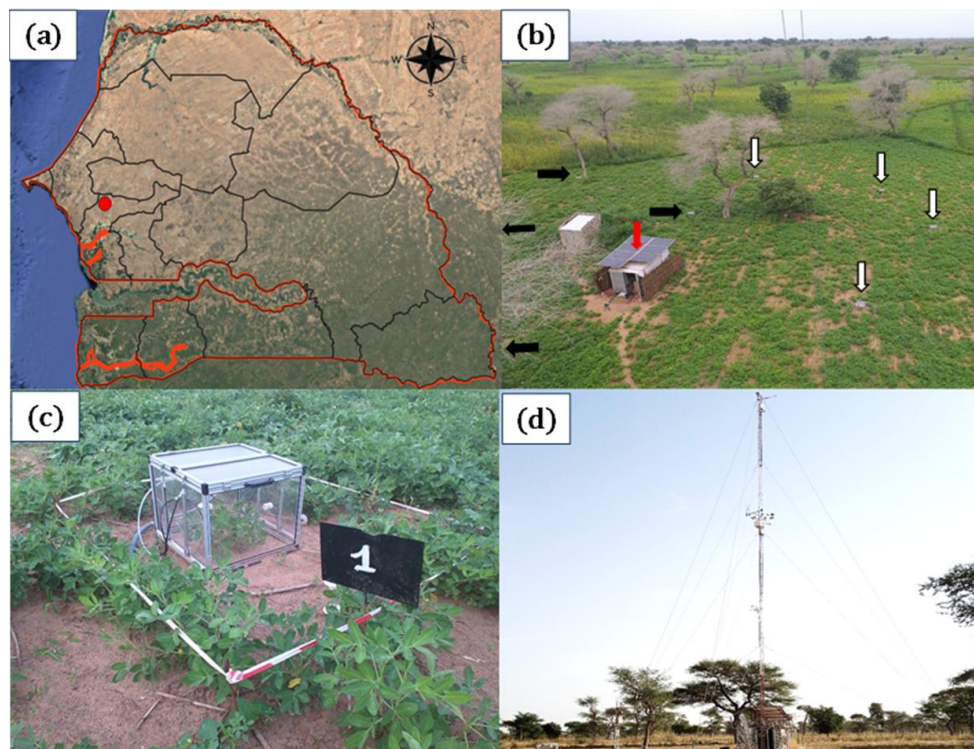
104 **2. Materials and methods**

105 *2.1. Site description*

106 The study was conducted in the agroforestry parkland of Sob village (Niakhar municipality, Fatick  
107 region), located in the groundnut basin of Senegal, within the Sahelo-Sudanian climatic zone of  
108 West Africa (Fig. 1). The climate is characterized by a long dry season (8–9 months) with high  
109 temperatures and strong diurnal variations, and a short rainy season from late June to mid-  
110 October (Delaunay et al., 2018).

111 Soils are locally known as “*Dior*” and classified as Arenosols (IUSS Working Group WRB, 2022).  
112 The topsoil has low organic matter (<1%) and phosphorus (<3 mg kg<sup>-1</sup>), a sandy texture (>85%  
113 sand), and an acidic pH (Malou et al., 2021; Siegwart et al., 2022). Rainfed agriculture  
114 predominates. The main cropping system includes pearl millet (*Pennisetum glaucum L.*) and  
115 groundnut (*Arachis hypogaea L.*) in biennial rotation, with occasional intercropping of cowpea  
116 (*Vigna unguiculata L.*).

117 The site hosts the 'Faidherbia Flux' station (14°29'44.916"N; 16°27'12.851"W; FLUXNET ID: SN-  
118 Nkr), a long-term research platform for monitoring ecosystem services in agroforestry systems.  
119 It is dominated by *F. albida*, a nitrogen-fixing, reverse-phenology tree with deep roots accessing  
120 groundwater (Roupsard et al., 1999). The tree density is ~13 trees ha<sup>-1</sup>, with canopies covering  
121 ~10% of the soil surface (Roupsard et al., 2020). The EC tower is installed at 20 m height,  
122 approximately 12.5 m above the canopy. The study field is a typical 'bush field', characterized by  
123 low soil fertility, no mineral fertilization, and off-site export of crop residues and manure (Malou  
124 et al., 2021).



125 Fig. 1: Study area.

126 (a) geographical location of Sob, Groundnut basin, Senegal (Map data © Google Earth, 2025), (b) overview  
127 (image from the Eddy Covariance tower located in the same bush-field) of the *Faidherbia albida* parkland  
128 during the rainy season, depicting groundnut crops with bare soil in the inter-row, *F. albida* trees  
129 (defoliated during the rainy season, average height = 13m) and location of the chambers under the Shade  
130 of trees (horizontal black arrows; N=4) and in Full sun (vertical white arrows; N=4); The shelter (red  
131 arrow) with solar panels is to fit the analyser, automation and batteries (c) automatic chamber enclosing a  
132 groundnut plant (during the rainy season) or bare soil (during the dry season), (d) Eddy Covariance (EC)  
133 tower (measurement height = 20 m) during the dry season.



134 *2.2. Experimental setup*

135 *2.2.1. CO<sub>2</sub> flux measurements in automatic chambers*

136 Continuous net CO<sub>2</sub> fluxes (FCO<sub>2</sub>ch) from soil and groundnut plants were measured over a full  
137 phenological year (June 17, 2021 – June 17, 2022) using eight automated static chambers  
138 (50×50×50 cm), each enclosing one groundnut plant. Four chambers were installed in full sun  
139 (FS), at least 20 m from trees, and four under *F. albida* canopy shade (Sh). The chambers were  
140 transparent, custom-built (Duthoit et al., 2020), and installed on metal bases embedded 10 cm  
141 into the soil one month prior to measurements.

142 During the rainy season (June–November), groundnut coexisted briefly with spontaneous weeds  
143 until weeding (mid-July), after which chambers contained only groundnut. Post-harvest (early  
144 November), chambers remained bare while surrounding plots experienced weed regrowth.

145 CO<sub>2</sub> concentrations were measured at 1 Hz using a Picarro G2508 gas analyser (Picarro Inc., Santa  
146 Clara, CA, USA) (Fleck et al., 2013; Reum et al., 2019; Valujeva et al., 2022). A fully automated  
147 system was built for sequential half-hour flux measurements (alternating FS and Sh).  
148 Measurement duration was 15 min per chamber in the dry season, reduced to 5 min during the  
149 rainy season to limit condensation effects.

150 *2.2.2. CO<sub>2</sub> flux measurements by Eddy Covariance*

151 The EC system (Li-COR SMARTFLUX®, including a Gill MasterPro 3D sonic anemometer and a LI-  
152 7500 RS open path CO<sub>2</sub> and H<sub>2</sub>O gas analyser) was mounted at a height of 20 m on a 30m mast,  
153 above *F. albida*. It continuously monitored net CO<sub>2</sub> exchange from the ecosystem. Raw data were  
154 collected at 20 Hz frequency and post-processed from binary files using the advanced mode of the  
155 EddyPro® v7.0, with standard corrections and procedures: sonic tilt correction (double rotation),  
156 block averaging, covariance maximisation for time lag, and WPL correction (Webb et al., 1980).  
157 Quality control followed Foken et al. (2004) and Vickers & Mahrt (1997); random uncertainty was  
158 estimated per Finkelstein & Sims (2001). Spectral corrections were applied according to  
159 Moncrieff et al. (1997, 2004). Footprints were computed according to Kormann and Meixner  
160 (2001), using the FREddyPro R package (Xenakis, 2016), indicated a ~1 ha source area covering  
161 the entire field. Gap-filling and flux partitioning were conducted using ReddyProc (Wutzler et al.,  
162 2018), applying the daytime partitioning approach of Lasslop et al. (2010).

163 *2.2.3. Ancillary measurements*

164 Environmental and vegetation variables were monitored continuously throughout the study.  
165 Global radiation (R<sub>g</sub>) was estimated from photosynthetically active radiation (PAR) using a Skye  
166 sensor (averaged over 30-min intervals). NDVI of crops under full sun was recorded semi-hourly



167 by a calibrated downward-facing sensor installed at 20 m height (Pontauiller et al., 2003),  
168 processed following Soudani et al. (2012), and used to estimate LAI time series for groundnut,  
169 weeds, and cowpea based on end-of-season field LAI measurements in six 15 m<sup>2</sup> plots (as in  
170 Roupsard et al., 2020).

171 Rainfall was recorded by an automatic weather station (CR1000 with TE525MM rain gauge,  
172 Campbell Scientific), and soil volumetric water content (VWC) and temperature ( $T_{\text{soil}}$ , at 6 cm  
173 depth) were monitored using TOMST® TMS-4 sensors, benchmarked prior to field deployment  
174 inside and outside the chambers (Wild et al., 2019). Air temperature ( $T_{\text{air}}$ ) was recorded inside  
175 each chamber at 15 cm above ground, all at 5-min intervals. These measurements contribute to  
176 the SoilTemp global database (Lembrechts et al., 2020, 2022).

177 Groundnut development was tracked weekly by counting leaves in each chamber. Total  
178 groundnut LAI (LAI<sub>ch</sub>) was then derived from average single-leaf area and chamber surface.

179 A detailed description of the data used in this study is provided in Supplement S1 (Table S1.1).

### 180 2.3. Data processing

#### 181 2.3.1. Flux calculation

182 Net CO<sub>2</sub> fluxes (FCO<sub>2</sub>ch, in μmol CO<sub>2</sub> m<sup>-2</sup> s<sup>-1</sup>) from the chambers were calculated from the linear  
183 change in CO<sub>2</sub> concentration over time ( $\Delta C/\Delta t$ ) using the Eq.1.

$$184 \text{FCO}_{2\text{ch}} = \left(\frac{P}{R T_k}\right) \left(\frac{V}{A}\right) \left(\frac{\Delta C}{\Delta t}\right) \quad (\text{Eq. 1})$$

185 where P is atmospheric pressure (101 325 N m<sup>-2</sup>), R is the ideal gas constant (8.31 N m mol<sup>-1</sup> K<sup>-1</sup>),  
186  $T_k$  is air temperature inside the chamber in Kelvin, V (0.125 m<sup>3</sup>) is the total system volume  
187 (chamber, tubing, analyser cavity, pump, and water trap), and A (0.25 m<sup>2</sup>) is the chamber  
188 footprint. The slope  $\Delta C/\Delta t$  was obtained via linear regression (Duthoit et al., 2020).

189 Mean FCO<sub>2</sub>ch values were computed separately for the four replicate chambers in full sun (FS)  
190 and under *F. albida* shade (Sh). By convention, negative values indicate net CO<sub>2</sub> uptake  
191 (photosynthesis), and positive values indicate net CO<sub>2</sub> release (respiration).

#### 192 2.3.2. Quality control of chamber-based CO<sub>2</sub> flux measurements

193 The quality of chamber-based CO<sub>2</sub> flux measurements was assessed using the coefficient of  
194 determination ( $R^2 \geq 0.8$ ) of the linear increase in CO<sub>2</sub> concentration during chamber closure. The  
195 minimum detectable flux (MDF) was then calculated following Nickerson (2016) (Eq.2). The MDF  
196 defines the flux detection threshold, below which data are considered unreliable due to  
197 instrument sensitivity and sampling constraints (Zaman et al., 2021). In this study, the MDF was  
198  $\pm 0.0004 \mu\text{mol CO}_2 \text{ m}^{-2} \text{ s}^{-1}$ .

199



200 
$$\mathbf{MDF} = \left( \frac{A_a}{t_c(\sqrt{t_c/p_s})} \right) \left( \frac{VP}{ART} \right) \quad \mathbf{(Eq. 2)}$$

201 where  $A_a$  is the analytical precision of the Picarro analyser (0.6 ppm; Picarro Inc., 2015),  $t_c$  the  
202 closure time (s),  $p_s$  the sampling frequency (1 Hz),  $V$  the chamber volume,  $P$  the atmospheric  
203 pressure (101 325 N m<sup>-2</sup>),  $A$  the chamber footprint,  $R$  the gas constant (8.3 N m mol<sup>-1</sup>·K<sup>-1</sup>), and  $T$   
204 the air temperature in Kelvin.

205 Following this quality control, fluxes were partitioned (Section 2.3.3) and gap-filled (Section  
206 2.3.4).

### 207 *2.3.3. Partitioning of chamber-based CO<sub>2</sub> fluxes*

208 The net CO<sub>2</sub> fluxes (FCO<sub>2</sub>ch), averaged from four chambers per environment (FS and Sh), were  
209 partitioned into two components according to Eq. 3 (Reichstein et al., 2005).

210 
$$\mathbf{FCO_2ch} = \mathbf{Rch} + \mathbf{GPPch} \quad \mathbf{(Eq. 3)}$$

211 Rch includes heterotrophic respiration (Rh) from soil and other autotrophic respiration (Ra) from  
212 groundnut plants and roots of *F. albida* (Ra Groundnut + Ra tree below-ground). Rch is always  
213 positive (Rch > 0). GPPch (Gross Primary Productivity) represents the photosynthetic CO<sub>2</sub> uptake  
214 by the groundnut plants and is negative during the day (GPPch < 0), and zero at night, when  
215 FCO<sub>2</sub>ch = Rch.

216 Half-hourly FCO<sub>2</sub>ch fluxes were partitioned as follows: (1) an Arrhenius-type function (Lloyd &  
217 Taylor, 1994) was fitted between nocturnal Rch and T<sub>soil</sub> during nighttime periods, for each 5-days  
218 throughout the time series (Eq. 4). This empirical formulation is based on several key  
219 assumptions. First, the relationship between nocturnal respiration and soil temperature is  
220 assumed to follow an exponential response, reflecting the temperature sensitivity of respiration  
221 processes. Second, the model assumes temporal stability of the respiration–temperature  
222 relationship between night and day, allowing diurnal respiration to be extrapolated from fitted  
223 parameters in Eq.4 and daytime T<sub>soil</sub>. Third, we assumed that no abrupt changes in substrate  
224 availability or soil moisture occur between day and night — conditions that could otherwise  
225 disrupt the temperature–respiration relationship. Third, it is assumed that no abrupt changes in  
226 substrate availability or soil moisture occur between night and day — conditions that could  
227 otherwise decouple respiration rates from temperature. These assumptions are widely applied in  
228 CO<sub>2</sub> flux partitioning approaches (Reichstein et al., 2005; Lasslop et al., 2010). (2) Diurnal Rch  
229 was estimated by applying the Lloyd & Taylor function, previously calibrated on nocturnal data,  
230 to the corresponding daytime T<sub>soil</sub> measurements for each 5-day interval. (3) GPPch was  
231 subsequently derived as the residual component of the net CO<sub>2</sub> flux during the day, according to:

232

233



234 **nocturnal Rch** =  $R_{\text{ref}} \cdot \exp \left[ E_0 \left( \frac{1}{T_{\text{ref}} - T_0} - \frac{1}{T_{\text{soil}} - T_0} \right) \right]$  (Eq. 4)

235 where  $R_{\text{ref}}$  ( $\mu\text{mol CO}_2 \text{ m}^{-2} \text{ s}^{-1}$ ) is a fitted parameter representing the base respiration at the  
236 reference temperature [ $T_{\text{ref}}$  (K), (set at 288.15 K)].  $E_0$  (K) is the temperature sensitivity (set at  
237 250 K),  $T_{\text{soil}}$  (K) the soil temperature (K), and  $T_0$  (K) is kept constant at 231.13 K, according to  
238 Lloyd & Taylor (1994).

239 **GPPch** = **diurnal FCO<sub>2</sub>ch** – **diurnal Rch** (Eq. 5)

240 where diurnal FCO<sub>2</sub>ch and diurnal Rch represent the daytime net CO<sub>2</sub> fluxes and respiration in  
241  $\mu\text{mol CO}_2 \text{ m}^{-2} \text{ s}^{-1}$ , respectively.

#### 242 2.3.4. Gap-filling procedure

243 Missing Rch data were gap-filled using the model derived from Eq. 4 (Lloyd & Taylor, 1994). Prior  
244 to gap-filling GPPch, raw data were standardised by LAI to reduce variability between chambers  
245 due to differences in leaf surface area (Eq. 6). A light-response model was then fitted to the  
246 standardised GPPch data, every 5-day period, to gap-fill missing values. The model is based on a  
247 rectangular hyperbolic function that describes the relationship between photosynthetic CO<sub>2</sub>  
248 uptake and incoming global radiation (Rg) (Eq. 7). It corresponds to a Michaelis–Menten-type  
249 light-response curve, commonly used in ecosystem carbon exchange studies (Falge et al., 2001;  
250 Lasslop et al., 2010).

251 **GPPch.stand** =  $\frac{\text{GPPch}}{\text{LAIch}} * \text{LAI.field}$  (Eq. 6)

252 where GPPch.stand ( $\mu\text{mol CO}_2 \text{ m}^{-2} \text{ s}^{-1}$ ) is the standardised GPPch. LAI<sub>ch</sub> and LAI<sub>field</sub> ( $\text{m}^2$  leaves  
253  $\text{m}^{-2}$  soil) represent the groundnut LAI inside the chambers and the groundnut + weeds + cowpea  
254 LAI for the whole field, respectively.

255 **GPP** =  $\frac{\alpha \beta R_g}{\alpha R_g + \beta}$  (Eq. 7)

256 where  $\alpha$  ( $\mu\text{mol CO}_2 \text{ J}^{-1}$ ) represents the light use efficiency of the groundnut plants inside the  
257 chambers, and refers to the initial slope of the light-response curve,  $\beta$  ( $\mu\text{mol CO}_2 \text{ m}^{-2} \text{ s}^{-1}$ ) is the  
258 maximum CO<sub>2</sub> uptake rate by the groundnut plants at light saturation, and Rg the global radiation  
259 ( $\text{W m}^{-2}$ ).

#### 260 2.3.5. Comparing chamber-based (Ch) and Eddy Covariance (EC) methods

261 Chamber measurements were upscaled to field-level CO<sub>2</sub> fluxes and compared with EC-derived  
262 fluxes. Before comparison, a correction was applied (Eq. 6) to account for differences in LAI  
263 between chambers (LAI<sub>ch</sub>) and the field (LAI<sub>field</sub>), due to the presence of cowpea and weeds in  
264 the field but not in the weeded chambers.

265 Upscaling considered tree cover, with FS and Sh chamber fluxes weighted at 90% and 10%,  
266 respectively. Rch.stand and GPPch.stand, representing chamber-based respiration and



267 photosynthesis at field scale. These fluxes were compared, on a half-hourly basis, to EC-derived  
268 Reco.EC and GPP.EC (S3, Table S3.1). The November–December transition period was excluded  
269 due to weed-driven uncertainties after groundnut harvest.

270 During the rainy season (*F. albida* leafless), GPP.EC represented ground vegetation (groundnut,  
271 cowpea, weeds), while Reco.EC included autotrophic respiration from all vegetation (including  
272 trees), and heterotrophic respiration (Reco.EC =  $R_a$  tree below-ground +  $R_a$  tree above-ground  
273 +  $R_a$  groundnut +  $R_a$  cowpea +  $R_a$  weeds +  $R_h$ ). Rch.stand could not be fully upscaled to the field  
274 due to uncertainty in its partitioning between  $R_a$  and  $R_h$ . Rch.stand accounted only for  $R_a$  tree  
275 below-ground,  $R_a$  groundnut, and  $R_h$ .

276 In the dry season (leafy trees, bare soil), GPP.EC reflected tree photosynthesis only (GPP tree),  
277 while GPPch.stand was nil. Reco.EC included  $R_a$  tree (above- and below-ground) and  $R_h$ .  
278 Rch.stand, measured on bare soil represented only  $R_a$  tree below-ground +  $R_h$ .

### 279 *2.3.6. Contribution of trees to full ecosystem respiration and photosynthesis*

280 During the dry season, when the trees (*F. albida*) maintained their foliage, a comparison between  
281 chamber and EC measurements allowed for the estimation of the contribution of the above-  
282 ground tree compartments to total ecosystem respiration (S3, Table S3.1). Based on this estimate,  
283 total tree respiration ( $R_a$  tree) was then calculated under the assumption that the tree root  
284 systems ( $R_a$  tree below-ground) represent  $\frac{1}{3}$  of the above-ground biomass (Jackson et al. 1996).  
285 Given the GPP measured during the dry season was equivalent to GPP of trees (GPP trees) from  
286 EC measurements, the carbon use efficiency of the trees (CUE tree) was then calculated (S3, Table  
287 S3.1). The resulting CUE value was assessed to determine whether it approximated the typical  
288 value of 0.5, which is often used as a default in ecosystem models (Zhou et al., 2019; 2020).

### 289 *2.3.7. Net annual C budget at the ASPS scale*

290 The annual C budget of  $\text{CO}_2$  fluxes was estimated for chambers and EC measurements in  $\text{Mg C-CO}_2$   
291  $\text{ha}^{-1}$ . The chambers  $\text{CO}_2$  fluxes budgets were obtained by calculating the annual sum of the net  
292  $\text{CO}_2$  flux measurements and then weighting with the tree cover rate (10% for the Sh, 90% for the  
293 FS). These annual budgets for the field are considered apparent, as they do not account for the  
294 biomass exported from the field after the harvest, the decomposition of which therefore escaped  
295 both the chambers and the EC. Additionally, the inputs and the outputs of fecal matter resulting  
296 from livestock wandering during the dry season were not quantified and are therefore neglected.  
297 The objective here is to compare two approaches at different scales using apparent net C budgets,  
298 rather than to provide an absolute C budget.



299 *2.4. Statistical analyses*

300 Statistical analyses were performed using the R software (R. Core Team, 2023). To compare the  
301 mean values of climatic parameters between the FS and Sh situations, a non-parametric Mann-  
302 Whitney test was used when both the normality (`shapiro.test`) and the homogeneity of the  
303 variance (Levene Test, R package ‘Car’; Fox et al., 2023) were not confirmed. This approach was  
304 similarly applied to compare the seasonal dynamics of CO<sub>2</sub> fluxes between FS and Sh, as well as  
305 between the chamber-based and Eddy Covariance (EC) methods. Means and standard deviations  
306 were computed using the ‘skim’ function from the R package ‘skimr’ (Waring et al., 2022).

307 Respiration (R<sub>ch</sub>) (Eq. 4) and GPP (GPP<sub>ch</sub>) models (Eq. 7) were fitted using non-linear least  
308 squares regression, implemented in the library in R ‘`nls.multstart`’ (Padfield et al., 2025). For the  
309 GPP<sub>ch</sub> model, parameters  $\alpha$  and  $\beta$  with non-significant p-values were removed, and then the  
310 remaining values were interpolated and smoothed using a ‘spline’ function from the ‘zoo’ library  
311 in R (Zeileis et al., 2024). Ordinary least-square linear regressions were fitted between the  
312 measured and the modeled values derived from. Model performance of Eq. 4 and Eq. 7 was  
313 evaluated by fitting ordinary least-square linear regressions between the measured and the  
314 modeled values using R<sup>2</sup>, root mean square error (RMSE), and the bias metrics. Given that the  
315 primary objective of these equations was to accurately reproduce the seasonal dynamics of the  
316 CO<sub>2</sub> fluxes to fill gaps in data, particular emphasis was placed on R<sup>2</sup>, with a higher value reflecting  
317 a better fit of the model to the measurements.

318 Correlation analysis was conducted between chamber CO<sub>2</sub> fluxes (FCO<sub>2ch</sub>, R<sub>ch</sub>, GPP<sub>ch</sub>) and soil  
319 temperature (T<sub>soil</sub>, °C), air temperature (T<sub>air</sub>, °C), VWC, the leaf area index of groundnut plants in  
320 the chambers (LAI<sub>ch</sub>), and the fitted parameters for respiration — R<sub>ref</sub> — and photosynthesis —  
321  $\alpha$  and  $\beta$ . This analysis was performed using the ‘`cor.test`’ function from the ‘stats’ package in R  
322 (Lüdecke et al., 2021), applying the Spearman method.

323 The threshold of the daily mean soil temperature (T<sub>soil</sub>, °C) at which the cumulative daily  
324 respiration (R<sub>ch</sub>, g C-CO<sub>2</sub> m<sup>-2</sup> d<sup>-1</sup>) began to decline was determined using segmented regression  
325 from the R package ‘segmented’ (Muggeo, 2003). The associated uncertainty (standard error) of  
326 this estimate was evaluated through a bootstrap procedure.

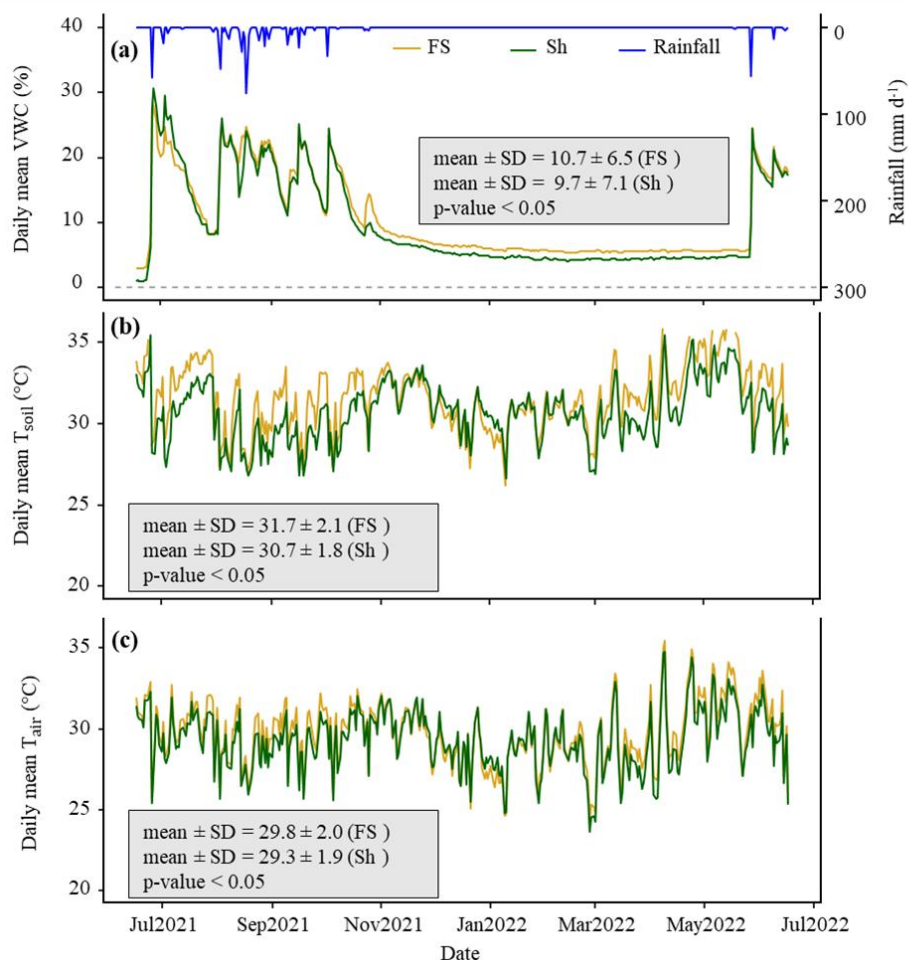


327 **3. Results**

328 *3.1. Microclimatic conditions*

329 During the experiment, the cumulative rainfall was 550 mm, which was representative of the  
330 interannual average. Precipitations were lowest in July and highest between August and  
331 September, a period that typically corresponds to the peak of the rainy season (Fig. 2a). Global  
332 radiation ranged between 5.8 and 32.4 MJ m<sup>-2</sup> d<sup>-1</sup> (data not shown). The daily mean VWC in the  
333 chambers showed significant variation, ranging from 1% at the end of the dry season to a  
334 maximum of 30% during the rainy season (Fig. 2a). While VWC was similar during the rainy  
335 season, it remained consistently higher in FS than in Sh throughout the dry season ( $p < 0.05$ ),  
336 which was unexpected. However, it should be noted that the last rain of October 2021 recharged  
337 the FS chambers more effectively, likely due to foliage rainfall interception by *F. albida* which had  
338 just put on leaves at that time, potentially explaining this discrepancy in VWC.

339 Within the chamber, the daily mean  $T_{\text{soil}}$  ranged from 26°C in April to 37.5°C at the end of the dry  
340 season (Fig. 2b), while  $T_{\text{air}}$  varied between 23.7°C and 35.5°C (Fig. 2c). However, during  
341 instantaneous daily peaks,  $T_{\text{soil}}$  could exceed 45°C in May (data not shown). As expected, both daily  
342 mean  $T_{\text{soil}}$  and  $T_{\text{air}}$  were significantly higher in FS compared to Sh situations ( $p < 0.05$ ), with  $T_{\text{soil}}$   
343 and  $T_{\text{air}}$  averaging respectively 1°C and 0.5°C lower under the tree canopy.



344 Fig. 2: One-year time series of daily average microclimatic parameters measured inside chambers.

345 (a) volumetric soil water content (VWC) at a depth of 6 cm (%). (b) soil temperature ( $T_{\text{soil}}$ ) at a depth of 6  
346 cm ( $^{\circ}\text{C}$ ), (c) air temperature ( $T_{\text{air}}$ ) at a height of 15 cm ( $^{\circ}\text{C}$ ). The blue line depicts the daily rainfall ( $\text{mm d}^{-1}$ )  
347 throughout the year. FS: Full sun chambers; Sh: Shaded chambers. Mean and SD represent respectively the  
348 mean value and the standard deviation. The p-value indicates the probability associated with the statistical  
349 test, assessing the differences in means between FS and Sh with the significance level  $\alpha$  set to 0.05.



350 *3.2. Modeling the chamber-based total respiration ( $R_{ch}$ ) and photosynthesis ( $GPP_{ch}$ )*

351 *3.2.1. Dynamics of references respiration, light use efficiency, and maximum  $CO_2$  uptake rate at*  
352 *light saturation ( $R_{ref}$ ,  $\alpha$ , and  $\beta$ )*

353 The reference respiration ( $R_{ref}$ ) showed comparable seasonal dynamics both at a distance from  
354 the trees (FS) and under the tree canopies (Sh) (S2, Fig. S2.2). In both situations,  $R_{ref}$  showed  
355 strong variability during the rainy season, peaking in September 2021 at  $2.4 \mu\text{mol CO}_2 \text{ m}^{-2} \text{ s}^{-1}$  for  
356 FS and  $2.9 \mu\text{mol CO}_2 \text{ m}^{-2} \text{ s}^{-1}$  for Sh (S2, Table S2.1). In contrast, during the dry season — from  
357 November 3, 2021 (after harvest) until the onset of the following rainy season (June 2022) —  $R_{ref}$   
358 values dropped both for FS and Sh, averaging  $0.3 \pm 0.5 \mu\text{mol CO}_2 \text{ m}^{-2} \text{ s}^{-1}$  for FS and  $0.5 \pm 0.6 \mu\text{mol}$   
359  $\text{CO}_2 \text{ m}^{-2} \text{ s}^{-1}$  for Sh. This represents a reduction by a factor of 8 for FS and 6 for Sh compared to the  
360 rainy season. The mean annual  $R_{ref}$  values were significantly higher under Sh than in FS, with value  
361 approximately 1.5 times greater (S2, Table S2.1).

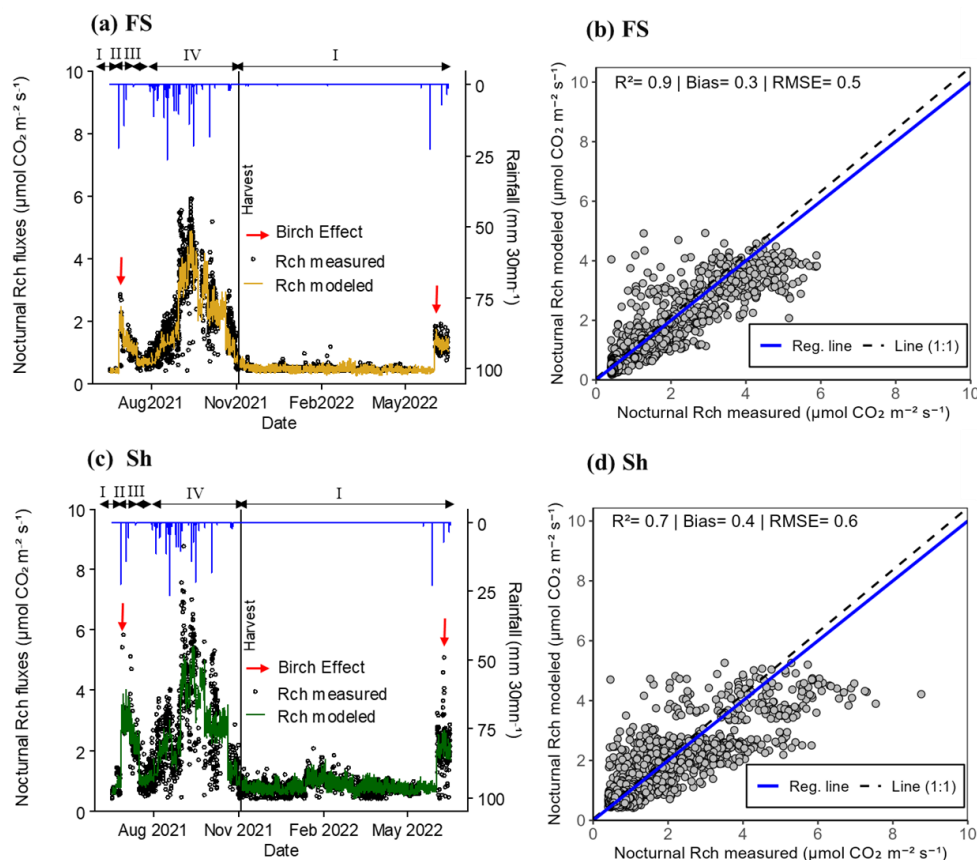
362 Regarding GPP in chambers, the light use efficiency ( $\alpha$ ) and the maximum  $CO_2$  uptake by  
363 groundnut plants in the chambers ( $\beta$ ), also reached their maximum during the peak of the rainy  
364 season (S2, Fig. S2.3, a and b). The maximum value of  $\alpha$  reached  $0.2 \mu\text{mol CO}_2 \text{ J}^{-1}$  in FS and  $0.3$   
365  $\mu\text{mol CO}_2 \text{ J}^{-1}$  in Sh (S2, Table S2.1). Similarly, the maximum values of optimum  $CO_2$  uptake rate at  
366 light saturation ( $\beta$ ) were  $40.2 \mu\text{mol CO}_2 \text{ m}^{-2} \text{ s}^{-1}$  for FS and  $42.8 \mu\text{mol CO}_2 \text{ m}^{-2} \text{ s}^{-1}$  for Sh (S2, Table  
367 S2.1). In the dry season, when photosynthetic activity ceased in the chambers, both  $\alpha$  and  $\beta$  were  
368 assumed to be nil (S2, Fig. S2.3, a and b). On average,  $\alpha$  and  $\beta$  were significantly higher in Sh than  
369 in FS, by a factor of 1.7 and 1.2, respectively (S2, Table S2.1). We noted that the decline in  
370 photosynthetic activity of the groundnut crop occurred earlier and rapidly at a distance from the  
371 trees (FS), as reflected by the sharply observed recession of  $\alpha$  and  $\beta$  in FS.

372 *3.2.2. Dynamics of nocturnal respiration in chambers*

373 The averaged nocturnal respiration (nocturnal  $R_{ch}$ ) calculated from the measurements across  
374 each treatment (FS and Sh), showed similar seasonal patterns (Fig. 3, a and c). Following the first  
375 rains,  $R_{ch}$  values increased dramatically, with a nocturnal 'Birch effect' — a sudden pulse of  $CO_2$   
376 release following soil rewetting — observed to be more pronounced under Sh compared to FS,  
377 approximately by a factor of 2. At the peak of the rainy season (September), the maximum  
378 nocturnal  $R_{ch}$  values reached approximately  $6.0 \mu\text{mol CO}_2 \text{ m}^{-2} \text{ s}^{-1}$  in FS and  $9.0 \mu\text{mol CO}_2 \text{ m}^{-2} \text{ s}^{-1}$   
379 in Sh (Fig. 3, a and c). Thereafter, nocturnal  $R_{ch}$  declined well before the groundnut harvest along  
380 with the rainfall spacing and the groundnut crop senescence (data not shown). During the dry  
381 season nocturnal  $R_{ch}$  continued to decrease, with maximum values around  $1.0 \mu\text{mol CO}_2 \text{ m}^{-2} \text{ s}^{-1}$   
382 in FS and  $2.0 \mu\text{mol CO}_2 \text{ m}^{-2} \text{ s}^{-1}$  in Sh (Fig. 3, a and c).



383 The modeled nocturnal Rch values closely matched the measured nocturnal Rch values (mean  
384 across four chambers per treatment), as indicated by the model performance metrics ( $R^2 = 0.9$ ,  
385 with bias and RMSE values of 0.3 and  $0.5 \mu\text{mol CO}_2 \text{ m}^{-2} \text{ s}^{-1}$ , respectively, for FS;  $R^2 = 0.7$ , with bias  
386 and RMSE values of 0.4 and  $0.6 \mu\text{mol CO}_2 \text{ m}^{-2} \text{ s}^{-1}$ , respectively, for Sh) (Fig. 3, b and d). Similarly,  
387 the daily mean modeled values also fitted well with the measured values, with FS showing  $0.9 \pm$   
388  $0.9 \mu\text{mol CO}_2 \text{ m}^{-2} \text{ s}^{-1}$  (modeled) and  $1.2 \pm 1.2 \mu\text{mol CO}_2 \text{ m}^{-2} \text{ s}^{-1}$  (measured), while Sh recorded  
389  $1.4 \pm 0.9 \mu\text{mol CO}_2 \text{ m}^{-2} \text{ s}^{-1}$  (modeled) and  $1.5 \pm 1.2 \mu\text{mol CO}_2 \text{ m}^{-2} \text{ s}^{-1}$  (measured). Given the close  
390 match between the measured and modeled values, the fitted model parameters were used  
391 subsequently to fill data gaps and estimate diurnal Rch values, as presented in Fig. 4, a and c.



392 Fig. 3: Dynamics of instantaneous nocturnal CO<sub>2</sub> fluxes in chambers in Full sun (FS; a and b) and  
 393 Shaded (Sh; c and d) environments (data filtered based on R<sup>2</sup> of the CO<sub>2</sub> variation over the time  
 394 of chamber closure and Minimum Detectable Flux, Eq.2).

395 (a) and (c): measured nocturnal respiration in chambers (Rch: black dots; average of measurements in 4  
 396 chambers per location) vs. modeled (coloured line). The vertical black line indicates the harvest date of  
 397 groundnuts inside the chambers. The red arrows indicate the 'Birch' effect and the blue line represents the  
 398 rainfall (mm 30mn<sup>-1</sup>). Roman numerals (above the black arrows) refer to vegetation conditions prevailing  
 399 inside the chambers, i.e. (I) bare soil, (II) weeds, (III) weeds + groundnuts, and (IV) groundnuts only.

400 (b) and (d): scatter plot between measured and modeled nocturnal Rch. The solid blue line indicates the  
 401 regression line and the dashed black one the (1:1) line RMSE and bias are expressed as fluxes (in µmol CO<sub>2</sub>  
 402 m<sup>-2</sup> s<sup>-1</sup>). Each point represents the mean value from 4 chambers within the FS or Sh environments.

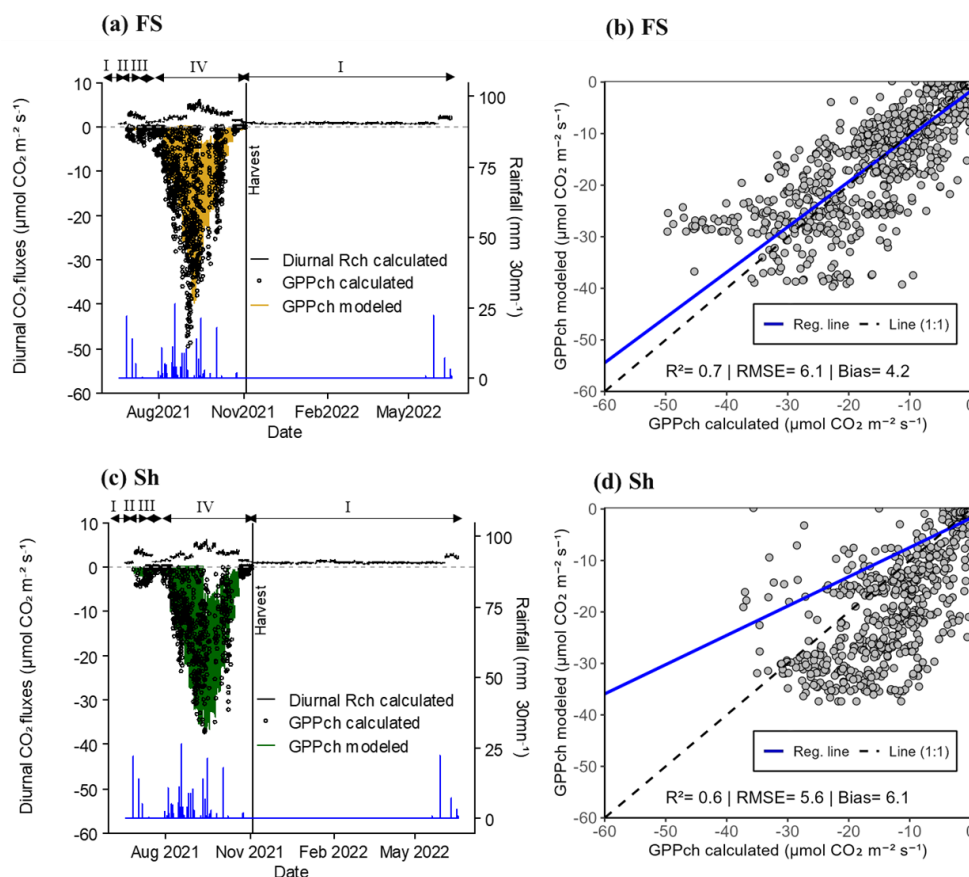


403 *3.2.3. Dynamics of daytime fluxes in chambers*

404 The measured GPP<sub>ch,stand</sub>, as well as GPP modeled with Eq. 6, showed similar seasonal dynamics  
405 in FS and Sh (Fig. 4, a and c). The fluxes peaked during the rainy season (Fig. 4a and c), coinciding  
406 with periods of vigorous vegetative growth characterised by a high leaf area index (LAI<sub>ch</sub>) of  
407 groundnut plants within the chambers (S2, Fig. S2.1). The maximum calculated and standardised  
408 GPP<sub>ch</sub> values reached  $-50 \mu\text{mol CO}_2 \text{ m}^{-2} \text{ s}^{-1}$  for FS and  $-37 \mu\text{mol CO}_2 \text{ m}^{-2} \text{ s}^{-1}$  for Sh. As expected,  
409 these fluxes were nil during the dry season when the soil was bare (Fig. 4, a and c).

410 The modeled GPP<sub>ch</sub> values closely followed the same trends as the calculated values, although  
411 model performance was slightly better for FS ( $R^2 = 0.7$  with bias and RMSE values of 4.2 and 6.1  
412  $\mu\text{mol CO}_2 \text{ m}^{-2} \text{ s}^{-1}$ , respectively) compared to Sh ( $R^2 = 0.6$  with bias and RMSE values of 6.1 and  
413  $5.6 \mu\text{mol CO}_2 \text{ m}^{-2} \text{ s}^{-1}$ , respectively) (Fig. 4, b and d).

414 The calculated diurnal respiration values (diurnal R<sub>ch</sub> calculated) for FS and Sh revealed a 'Birch  
415 effect' similar to that observed during the night, though slightly more pronounced under Sh by a  
416 factor of 1.2. Diurnal R<sub>ch</sub> values increased significantly during the rainy season, reaching a  
417 maximum of  $6.0 \mu\text{mol CO}_2 \text{ m}^{-2} \text{ s}^{-1}$  for both FS and Sh (Fig. 4, a and c). In the dry season, on bare  
418 soil, these values declined, with maximum respiration reaching only  $0.5 \mu\text{mol CO}_2 \text{ m}^{-2} \text{ s}^{-1}$  for both  
419 situations (FS and Sh) (Fig. 4, a and c).



420 Fig. 4: Dynamics of instantaneous diurnal CO<sub>2</sub> fluxes in chambers in Full sun (FS; a and b) and  
 421 Shaded (Sh; b and d) environments (filtered based on R<sup>2</sup> of the CO<sub>2</sub> variation over the time closure  
 422 in FS and Sh and Minimum Detectable Flux, Eq.2).

423 (a) and (c): non-gap-filled diurnal Rch calculated (black line, positive values; average of measurements in  
 424 4 chambers per location) and GPPch calculated from Eq.5 then standardised for LAI (black dots, negative  
 425 values) and modeled (coloured line, negative values). The vertical black line indicates the harvest date of  
 426 groundnuts inside the chambers and the blue line represents the rainfall (mm 30mn<sup>-1</sup>). Roman numerals  
 427 (above the black arrows) refer to conditions prevailing inside the chambers, i.e., (I) bare soil, (II) weeds,  
 428 (III) weeds + groundnuts, and (IV) groundnuts.

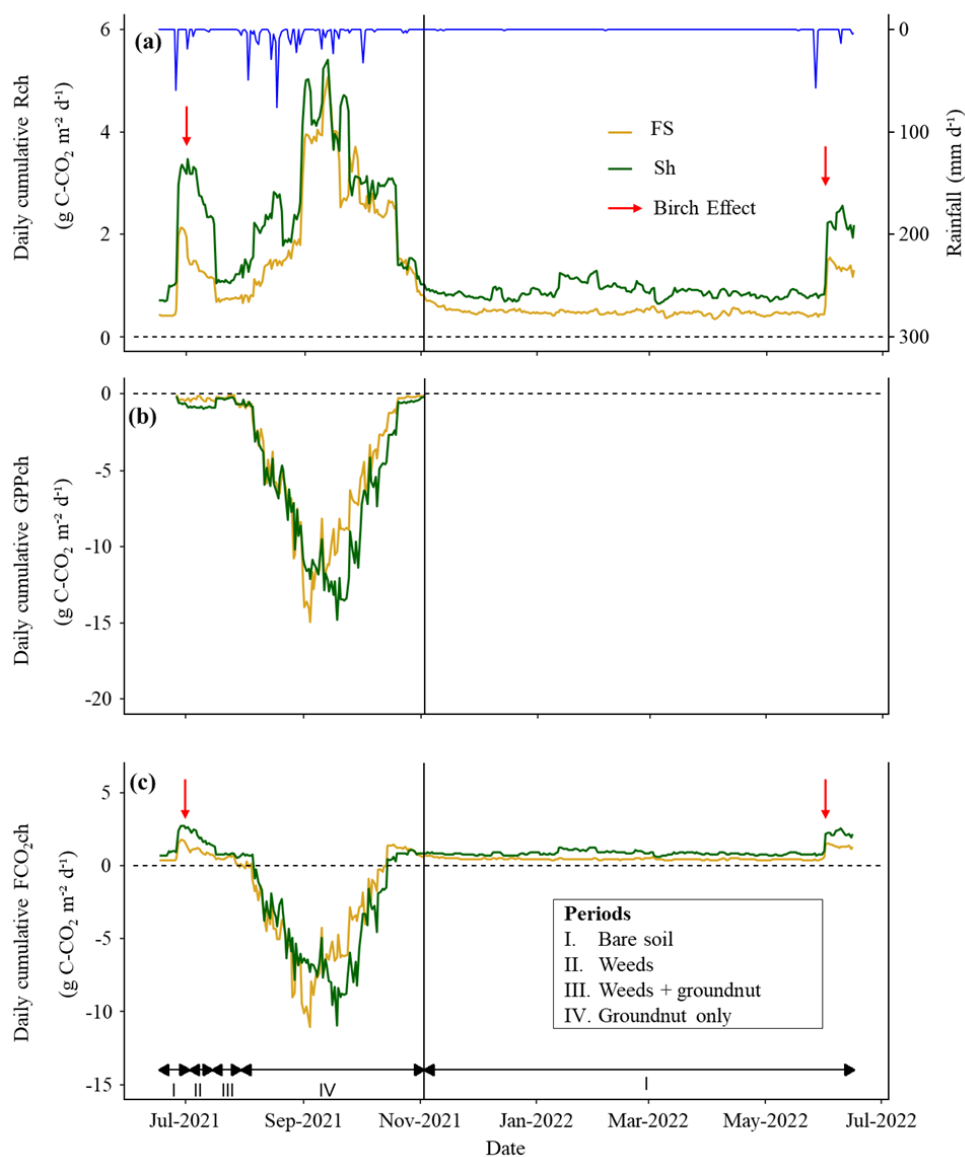
429 (b) and (d): scatter plot between calculated and modeled GPPch. The solid blue line indicates the regression  
 430 line and the dashed black one the (1:1) line. RMSE and bias are expressed as fluxes (in µmol CO<sub>2</sub> m<sup>-2</sup> s<sup>-1</sup>).  
 431 Each point represents the mean value from 4 chambers within the FS or Sh environments.



432 *3.3. Dynamics of daily cumulative CO<sub>2</sub> fluxes in chambers*

433 The seasonality of daily cumulative of GPPch.stand showed similar dynamics between FS and Sh,  
434 with higher variability during the rainy season than during the dry season (Fig. 5). Daily total Rch  
435 peaked during the rainy season at 5.1 g C-CO<sub>2</sub> m<sup>-2</sup> d<sup>-1</sup> for FS and 5.4 g C-CO<sub>2</sub> m<sup>-2</sup> d<sup>-1</sup> for Sh, while  
436 the maximum GPPch.stand values were comparable at around -15.0 g C-CO<sub>2</sub> m<sup>-2</sup> d<sup>-1</sup> for both FS  
437 and Sh (Table 1; S2, Fig. S2.4, a, b, c, and d). In the dry season, Rch decreased (Fig. 5), averaging  
438 0.5 g C-CO<sub>2</sub> m<sup>-2</sup> d<sup>-1</sup> for FS and 1.0 g C-CO<sub>2</sub> m<sup>-2</sup> d<sup>-1</sup> for Sh. GPPch declined well before harvest  
439 (senescence) and remained nil during the dry season (Fig. 5). During the rainy season FCO<sub>2</sub>ch  
440 peaked at around 11.0 g C-CO<sub>2</sub> m<sup>-2</sup> d<sup>-1</sup> for FS and Sh (Fig. 5) (Table 1; S2, Fig. S2.4, e and f), while  
441 FCO<sub>2</sub>ch values were the same as Rch during the dry season. In absolute terms, the mean Rch and  
442 GPPch were significantly higher under Sh as compared to FS, by factors of 1.3 and 1.2, respectively.  
443 Conversely, the mean FCO<sub>2</sub>ch was significantly higher under FS (0.4 g C-CO<sub>2</sub> m<sup>-2</sup> d<sup>-1</sup>) than under  
444 Sh (0.2 g C-CO<sub>2</sub> m<sup>-2</sup> d<sup>-1</sup>) (Table 1).

445 The annual cumulative Rch values were 392.8 g C-CO<sub>2</sub> m<sup>-2</sup> for FS and 574.5 g C-CO<sub>2</sub> m<sup>-2</sup> for Sh.  
446 The GPPch fluxes reached -539.5 g C-CO<sub>2</sub> m<sup>-2</sup> for FS and -632.6 g C-CO<sub>2</sub> m<sup>-2</sup> for Sh. Annual net  
447 cumulative C exchange (FCO<sub>2</sub>ch) were -146.7 g C-CO<sub>2</sub> m<sup>-2</sup> in FS and -58.1 g C-CO<sub>2</sub> m<sup>-2</sup> in Sh.



448 Fig. 5: Seasonal dynamics of daily gap-filled cumulative fluxes (in  $\text{gC-CO}_2 \text{ m}^{-2} \text{ d}^{-1}$ ) in chambers.

449 (a) soil+crop respiration (Rch), (b) photosynthesis (GPPch, standardised for LAI) and (c) net  $\text{CO}_2$  exchange  
 450 ( $\text{FCO}_{2\text{ch}}$ ). The yellow and green solid lines compare the FS and Sh environments, respectively. The vertical  
 451 black line indicates the harvest date of groundnuts inside the chambers. The blue line depicts the daily  
 452 cumulative rainfall ( $\text{mm d}^{-1}$ ) throughout the rainy season, and the red arrow indicates the 'Birch'  
 453 effect. Roman numerals (above the black arrows) in (a) and (c) refer to the prevailing conditions inside the  
 454 chambers: (I) bare soil, (II) weeds, (III) weeds + groundnuts, (IV) groundnuts.

455



456 Table 1: Comparison of daily cumulative and gap-filled chamber CO<sub>2</sub> fluxes (Rch, GPPch  
457 standardised for LAI, and FCO<sub>2</sub>ch in g C-CO<sub>2</sub> m<sup>-2</sup>) in the FS and Sh condition.

458

	Annual sum	Daily Mean ±SD	Min	Max	Mann-Whitney test
(g C-CO <sub>2</sub> m <sup>-2</sup> )	.yr <sup>-1</sup>	.d <sup>-1</sup>	.d <sup>-1</sup>	.d <sup>-1</sup>	
<b>Rch</b>					
FS	392.8	1.1 ± 0.9	0.4	5.1	*
Sh	574.5	1.6 ± 1.1	0.6	5.4	
<b>GPPch</b>					
FS	-539.5	-4.1 ± 4.3	< -0.1	-14.9	*
Sh	-632.6	-4.8 ± 4.6	< -0.1	-14.8	
<b>FCO<sub>2</sub>ch</b>					
FS	-146.7	-0.4 ± 2.4	-11.0	1.8	*
Sh	-58.1	-0.2 ± 2.7	-10.9	2.8	

459 Annual sum corresponds to the annual cumulative fluxes (g C-CO<sub>2</sub> m<sup>-2</sup> yr<sup>-1</sup>). Mean, SD, Min, and Max  
460 represent respectively the mean, standard deviation, minimum, and maximum values at the daily scale (g  
461 C-CO<sub>2</sub> m<sup>-2</sup> d<sup>-1</sup>). Asterisks (\*) indicate the p-values from the Mann-Whitney test, used to assess differences in  
462 mean between FS and Sh (p < 0.05). Positive values indicate CO<sub>2</sub> emissions, while negative values represent  
463 CO<sub>2</sub> uptake.



464 *3.4. Drivers of daily respiration and photosynthesis in chambers*

465 The chamber-based daily cumulative respiration (Rch) and GPPch showed significant and positive  
466 correlations with the leaf area index (LAIch), both at a distance from the trees (FS) and under the  
467 trees (Sh) (Table 2). The influence of LAIch on GPPch was stronger ( $r = 0.86$  for FS and Sh) than  
468 its influence on Rch ( $r = 0.60$  for FS;  $r = 0.69$  for Sh). Soil VWC was also positively correlated with  
469 Rch and GPPch, both in FS and Sh. However, the influence of soil VWC on Rch was stronger under  
470 Sh compared to FS, while its influence on GPPch was similar in both situations (FS and Sh). Soil  
471 temperature showed weak negative correlations with Rch (in FS and Sh) and with GPPch (only in  
472 Sh). Finally, no significant correlations were found between  $T_{air}$  and any of the CO<sub>2</sub> fluxes (Table  
473 2).



474 Table 2: Spearman correlation matrix based on daily cumulative and gap-filled CO<sub>2</sub> fluxes from full  
475 year chamber measurements (g C-CO<sub>2</sub> m<sup>-2</sup> d<sup>-1</sup>) with microclimatic parameters.

Parameters	Condition	Rch	GPPch
T <sub>soil</sub>	FS	-0.25 ***	ns
	Sh	-0.28 ***	-0.38 ***
T <sub>air</sub>	FS	ns	ns
	Sh	ns	ns
VWC	FS	0.51 ***	0.75 ***
	Sh	0.78 ***	0.75***
LAIch	FS	0.60 ***	0.86 ***
	Sh	0.69 ***	0.86 ***

476 Spearman correlation coefficients between daily cumulative and gap-filled CO<sub>2</sub> flux components (Rch and  
477 GPPch, with GPPch in absolute terms) and daily mean microclimatic parameters in full sun (FS) and shaded  
478 chambers (Sh). T<sub>soil</sub> (°C) is the daily mean soil temperature at 6 cm depth, T<sub>air</sub> (°C) the daily mean air  
479 temperature at 15 cm height, VWC (%) the daily mean volumetric water content (VWC, %), and LAIch (m<sup>-2</sup>  
480 leaf m<sup>-2</sup> soil) the chamber leaf area index value for a given day. Significance levels are indicated by (\*\*\*) for  
481 p < 0.001; ns denotes a non-significant correlation (p > 0.05)



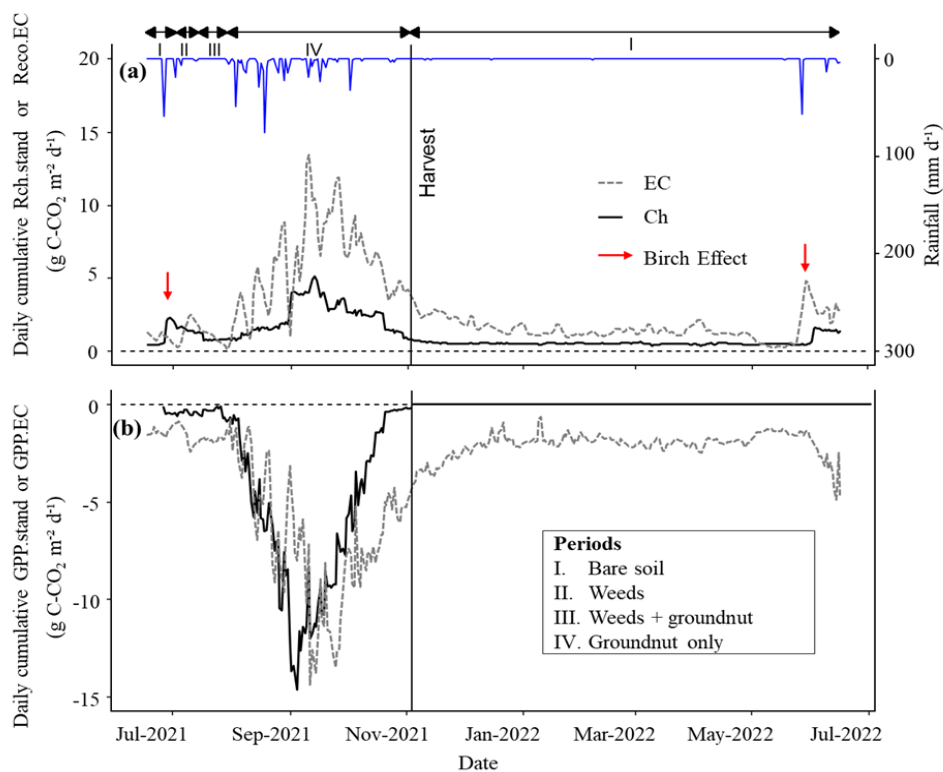
482 *3.5. Comparison of respiration and GPP measurements between chambers (Ch) and Eddy*  
483 *Covariance (EC) methods*

484 The chamber-based daily total CO<sub>2</sub> fluxes, gap-filled and weighted according tree cover were  
485 compared with the fluxes obtained using the EC method (Fig. 6).

486 During the rainy season, both total respiration and GPP showed comparable dynamics between  
487 the two methods, with synchronised peaks and higher variability compared to the dry season (Fig.  
488 6). The maximum value of Reco.EC, peaked at 13.5 g C-CO<sub>2</sub> m<sup>-2</sup> d<sup>-1</sup> (Table 3). The initial value of  
489 Rch.stand was comparable to Reco.EC but peaked only at 5.1 g C-CO<sub>2</sub> m<sup>-2</sup> d<sup>-1</sup> (Table 3), meaning  
490 a third of the peak of Reco.EC. The maximum GPP, was -14.3 g C-CO<sub>2</sub> m<sup>-2</sup> d<sup>-1</sup> and -14.6 g C-CO<sub>2</sub>  
491 m<sup>-2</sup> d<sup>-1</sup> for GPP.EC and GPPch.stand, respectively (Table 3). This indicates that the LAI-based  
492 standardisation and upscaling approach were realistic, at least up to the peak of groundnut  
493 growth.

494 On average, Reco.EC was significantly higher than Rch.stand, by a factor of 2.3. GPP.EC was also  
495 significantly higher than GPPch.stand, but only by a factor of 1.2 (Table 3).

496 During the dry season, Reco.EC and Rch.stand gradually decreased. The values for Reco.EC  
497 remained higher than for Rch.stand, which was fairly consistent with the contribution of the Ra  
498 tree above-ground compartment, even if this difference seemed to disappear at the end of the dry  
499 season (Fig. 6). The measured 'Birch effect' was highest for Rch.stand in 2021, but was the  
500 opposite in 2022 due to a system failure at the beginning of the rainy season. The maximum value  
501 of GPP.EC reached -2.4 g C-CO<sub>2</sub> m<sup>-2</sup> d<sup>-1</sup> when the trees were at their maximum of foliage, after  
502 harvest and while weeds were still present in the field. However, after the harvest, chamber  
503 photosynthesis (GPPch.stand) was nil (Table 3).



504 Fig 6: Comparing the seasonal dynamics of CO<sub>2</sub> fluxes between Eddy Covariance (EC)  
 505 measurements and upscaled chamber measurements (ch.stand).

506 (a) represent the seasonal dynamics of soil + crop respiration (Rch.stand) and ecosystem respiration  
 507 (Reco.EC) and (b) photosynthesis (GPP.stand and GPP.EC). The black and dashed grey lines show Ch and  
 508 EC seasonal dynamics, respectively. The vertical black line indicates the harvest date of groundnuts inside  
 509 the chambers. The blue line depicts the daily cumulative rainfall (mm d<sup>-1</sup>), and the red arrow indicates the  
 510 'Birch' effect. Roman numerals (above the black arrows) refer to conditions prevailing inside the  
 511 chambers: (I) bare soil, (II) weeds, (III) weeds + groundnuts, (IV) groundnuts.



512 Table 3: Comparison of gap-filled CO<sub>2</sub> fluxes between Eddy Covariance (EC) and upscaled chamber (Ch.stand) measurements, by season (rainy or dry).

	Rainy season					Dry season				
	Daily Mean ± SD .d <sup>-1</sup>	Min .d <sup>-1</sup>	Max .d <sup>-1</sup>	Mann-Whitney test	Daily Mean ± SD .d <sup>-1</sup>	Min .d <sup>-1</sup>	Max .d <sup>-1</sup>	Mann-Whitney test		
<b>(g C-CO<sub>2</sub> m<sup>-2</sup>)</b>										
<b>Reco.EC or Rch.stand</b>										
EC	4.6 ± 3.2	0.2	13.5	*	1.2 ± 0.4	0.3	2.1	*		
Ch.stand	2.0 ± 1.1	0.5	5.1		0.5 ± 0.04	0.4	0.6			
<b>GPP.EC or GPPch.stand</b>										
EC	-5.1 ± 3.6	-0.7	-14.3	*	-1.7 ± 0.3	-0.6	-2.4			
Ch.stand	-4.2 ± 4.3	<-0.1	-14.6		0	0	0			

513 Mean, SD, Min, and Max represent the daily mean fluxes, standard deviation, minimum, and maximum values, respectively (g C-CO<sub>2</sub> m<sup>-2</sup> d<sup>-1</sup>). The Asterisks (\*) indicate  
 514 the p-values from the Mann-Whitney test, used to assess differences in mean between EC and Ch. Positive values indicate CO<sub>2</sub> emissions, while negative values  
 515 represent CO<sub>2</sub> uptake.



516 *3.6. The contribution of F. albida to Reco and GPP*

517 During the dry season, the cumulative contribution of *F. albida* to ecosystem respiration (Ra tree)  
518 was 139.6 g C-CO<sub>2</sub> m<sup>-2</sup>. This represent 12% of the total annual cumulative Reco, which was  
519 estimated at 1180.0 g C-CO<sub>2</sub> m<sup>-2</sup>. The contribution of trees (GPP tree) to total annual GPP was -  
520 270.2 g C-CO<sub>2</sub> m<sup>-2</sup>, equivalent to ~50% of the total annual cumulative GPP of the ecosystem (550  
521 g C-CO<sub>2</sub> m<sup>-2</sup>).

522 The ratio between these two components (Ra tree / GPP tree) in absolute terms was 0.52,  
523 reflecting a carbon use efficiency (CUE) of 0.48 (S3, Table S3.1).

524 *3.7. Carbon budgets at the field-scale*

525 The upscaled chamber-based annual cumulative total respiration flux (Rch.stand) was estimated  
526 to be 4.1 ± 0.01 Mg C-CO<sub>2</sub> ha<sup>-1</sup> (Table 4). In comparison, the annual budget of Reco.EC was 10.0  
527 ± 0.03 Mg C-CO<sub>2</sub> ha<sup>-1</sup> (Table 4), more than two times larger than Rch.stand.

528 The upscaled GPPch.stand reached an annual cumulative value of -5.5 ± 0.03 Mg C-CO<sub>2</sub> ha<sup>-1</sup>,  
529 whereas the annual cumulative GPP.EC was -11.8 ± 0.03 Mg C-CO<sub>2</sub> ha<sup>-1</sup> (Table 4).

530 The annual net C budget, based on both methods, was estimated at -1.4 ± 0.02 Mg C-CO<sub>2</sub> ha<sup>-1</sup> for  
531 chambers (FCO<sub>2</sub>ch.stand) and -1.8 ± 0.01 Mg C-CO<sub>2</sub> ha<sup>-1</sup> for Eddy Covariance (NEE.EC) (Table 4).



532 Table 4: Annual budget of CO<sub>2</sub> fluxes based on Eddy Covariance (EC) and upscaled chamber  
533 methods (Ch.stand).

	Annual sum	Std error
	(Mg C-CO <sub>2</sub> ha <sup>-1</sup> )	(Mg C-CO <sub>2</sub> ha <sup>-1</sup> )
<b>Reco.EC or Rch.stand</b>		
EC	10.0	0.03
Ch.stand	4.1	0.01
<b>GPP.EC or GPPch.stand</b>		
EC	-11.8	0.03
Ch.stand	-5.5	0.03
<b>NEE.EC or FCO<sub>2</sub>ch.stand</b>		
EC	-1.8	0.01
Ch.stand	-1.4	0.02

534 Annual sum corresponds to the annual cumulative fluxes for full year measurements (Mg C-CO<sub>2</sub> ha<sup>-1</sup>). EC  
535 refers to fluxes measured by the Eddy Covariance method, and Ch refers to the fluxes measured by  
536 chambers, which are then upscaled to the whole field. Rch.stand represents the chamber respiration, while  
537 Reco.EC denotes the ecosystem respiration according to the EC method. GPP.EC and GPPch.stand are the  
538 gross primary production or photosynthesis flux, measured by EC and Ch methods, respectively. NEE.EC  
539 and FCO<sub>2</sub>ch.stand represent the net ecosystem exchange for EC and Ch, respectively. The associated  
540 standard error is denoted as Std error (Mg C-CO<sub>2</sub> ha<sup>-1</sup>). Positive values indicate CO<sub>2</sub> emissions, while  
541 negative values represent CO<sub>2</sub> uptake.



## 542 4. Discussion

### 543 4.1. Seasonality and drivers of chamber-based CO<sub>2</sub> fluxes

544 In our agroforestry context, seasonal variability in CO<sub>2</sub> fluxes closely followed rainfall dynamics,  
545 peaking during the wet season and declining sharply in the dry season, consistent with soil  
546 moisture depletion and crop senescence. This pattern is typical of semi-arid ecosystems (Ago et  
547 al., 2016a; Brümmer et al., 2008; Guillen-Cruz et al., 2023; Macharia et al., 2020; Mosongo et al.,  
548 2022; Wieckowski et al., 2024).

549 Respiration and photosynthesis were primarily driven by soil moisture and LAI, reflecting the  
550 system's sensitivity to water availability and crop dynamics. Soil moisture enhanced both  
551 processes by stimulating microbial activity and supporting plant growth (Borken et al., 2002;  
552 Conant et al., 2004; Merbold et al., 2009; Yu et al., 2020; Zhao et al., 2016). The stronger correlation  
553 between soil moisture and respiration under F. albida canopy (Sh:  $r = 0.78$ ) compared to full sun  
554 (FS:  $r = 0.51$ ) suggests greater microbial sensitivity to moisture beneath trees. This likely reflects  
555 enhanced substrate availability, resulting in stronger post-rainfall respiration pulses (Meisner et  
556 al., 2015) and supporting the 'fertile island' effect, where trees improve local soil conditions  
557 (Eldridge et al., 2024). Photosynthetic capacity also responded to soil moisture, as shown by  
558 positive correlations with LAI and key physiological traits such as light use efficiency ( $\alpha$ ) and  
559 maximum CO<sub>2</sub> uptake rate ( $\beta$ ) (Gonsamo et al., 2019; Qiu et al., 2023; Zhang et al., 2024).

560 In contrast, the influence of soil temperature ( $T_{\text{soil}}$ ) on respiration was weakly negative in both FS  
561 and Sh, indicating a thermal threshold beyond which respiration is suppressed—estimated at  $32$   
562  $\pm 1.5$  °C in FS and  $29.5 \pm 1.9$  °C in Sh (S2, Fig. S2.6, a and b), similar to findings in Eastern Ghana  
563 (Owusu et al., 2024). This inhibition likely results from decreased enzymatic and microbial  
564 activity under combined heat and water stress (Liu et al., 2018; Richardson et al., 2012). In semi-  
565 arid regions, soil respiration often becomes decoupled from temperature due to seasonal  
566 moisture constraints (Jia et al., 2020; Tucker & Reed, 2016; Warren, 2014), with microbial activity  
567 limited during dry periods despite favourable temperatures. This decoupling helps explain the  
568 weak or absent correlation between  $T_{\text{soil}}$  and soil moisture (S2, Fig. S2.5, b), particularly under Sh  
569 ( $r = -0.28$ ). Management practices such as organic inputs can also modulate these dynamics,  
570 adding further variability to soil respiration responses (Meena et al., 2020; Oyonarte et al., 2012;  
571 Rong et al., 2015; Xue & Tang, 2018).

### 572 4.2. Magnitude of chamber-based total CO<sub>2</sub> respiration fluxes

573 Mean total soil respiration values were consistent with those reported in other low-input  
574 agricultural systems across sub-Saharan Africa (Mapanda et al., 2010; Pelster et al., 2017;  
575 Rosenstock et al., 2016). In full sun (FS), the mean respiration ( $1.0 \pm 0.9$  g C-CO<sub>2</sub> m<sup>-2</sup> d<sup>-1</sup>) closely



576 matched values measured by Wachiye et al. (2020) in a semi-arid Kenyan field at 1158 m altitude  
577 ( $1.1 \pm 0.1$  g C-CO<sub>2</sub> m<sup>-2</sup> d<sup>-1</sup>). This similarity likely reflects comparable environmental conditions,  
578 including moderate rainfall (~550 mm yr<sup>-1</sup>) and low soil organic carbon and nitrogen contents  
579 (<1%) in the 0–20 cm layer of sandy soil. In contrast, respiration under *F. albida* canopy (Sh:  $1.6$   
580  $\pm 1.1$  g C-CO<sub>2</sub> m<sup>-2</sup> d<sup>-1</sup>) was higher, likely due to additional autotrophic respiration from tree roots  
581 and greater organic inputs beneath the canopy. Nonetheless, this flux remains close to values  
582 observed in low-input sorghum fields on sandy loam soils in eastern Ghana ( $1.7 \pm 1.1$  g C-CO<sub>2</sub> m<sup>-2</sup>  
583 d<sup>-1</sup>), despite higher rainfall (950–1000 mm yr<sup>-1</sup>) in that region (Owusu et al., 2024).

584 Cumulative annual respiration fluxes fell within the range reported for Sahelian croplands (250–  
585 450 g C-CO<sub>2</sub> m<sup>-2</sup>) (Brümmer et al., 2009) and other sub-Saharan African agricultural systems (Kim  
586 et al., 2016). The cumulative flux under tree cover is similar to that measured in cassava fields in  
587 eastern Tanzania (440 g C-CO<sub>2</sub> m<sup>-2</sup> yr<sup>-1</sup>), despite the latter receiving higher rainfall (~1115 mm  
588 yr<sup>-1</sup>) (Rosenstock et al., 2016). This convergence may stem from comparable soil fertility  
589 constraints, with low soil organic carbon (1–1.7%) and nitrogen contents (<0.5%). In contrast,  
590 the slightly lower cumulative flux in FS may reflect less favourable microclimatic conditions—  
591 such as elevated soil temperatures and increased aridity away from tree cover—limiting  
592 microbial activity (see Section 4.1).

593 Across sub-Saharan Africa, soil respiration fluxes based on static chamber measurements show  
594 high spatial variability, largely shaped by climate and land use. For example, Owusu et al. (2024)  
595 found higher respiration in woodlands ( $3.8 \pm 0.8$  g C-CO<sub>2</sub> m<sup>-2</sup> d<sup>-1</sup>) and grazed areas ( $2.7 \pm 1.7$ )  
596 than in croplands ( $1.7 \pm 1.1$ ) in humid eastern Ghana. This gradient was linked to differences in  
597 soil moisture and organic matter. Similarly, Rosenstock et al. (2016) reported much higher fluxes  
598 in highland pastures in Kenya (3.8–4.4 g C-CO<sub>2</sub> m<sup>-2</sup> d<sup>-1</sup>) compared to cultivated fields in eastern  
599 Tanzania ( $1.2 \pm 0.2$ ), highlighting the role of vegetation cover and soil fertility.

#### 600 4.3. Effect of trees on chamber-based soil respiration and photosynthesis

601 A notable increase in respiration and photosynthesis fluxes was observed under *F. albida* trees  
602 (Sh) compared at a distance from trees (FS). This increase may indicate the potential role of *F.*  
603 *albida* in modulating CO<sub>2</sub> exchange dynamics (Rch and GPPch) within this agro-silvo-pastoral  
604 system. These results are consistent with preliminary findings from similar environments  
605 (Duthoit et al., 2020).

606 Numerous studies have investigated the effect of tree species on greenhouse gas fluxes,  
607 particularly CO<sub>2</sub>, revealing significant variations across different ecological contexts (Bréchet et  
608 al., 2021, 2025; Klaus et al., 2024; Mazza et al., 2021; Ramesh et al., 2013; Rheault et al., 2024).  
609 However, the underlying mechanisms by which trees influence these dynamics are not yet fully  
610 understood.



611 In general, agroforestry systems have been well-documented for their ability to provide a range  
612 of ecosystem services (e.g., Assefa et al., 2024; Bado et al., 2021; Kuyah et al., 2019; Rolo et al.,  
613 2023). Specifically, *Faidherbia*-based agroforestry systems may play a crucial role in regulating  
614 CO<sub>2</sub> exchanges between the soil and atmosphere. *F. albida*-based agroforestry systems are  
615 recognized for enhancing both soil organic and mineral fertility (Bayala et al., 2020; Dilla et al.,  
616 2019; Sileshi, 2016; Sileshi et al., 2020; Stephen et al., 2020), mainly through litter accumulation  
617 and direct inputs from livestock excreta under their canopies. Additionally, the extensive roots  
618 system of *F. albida* trees helps concentrate mineral nutrients, contributing to the formation of a  
619 'fertile island' effect under the trees (Siegwart et al., 2022; Eldridge et al., 2024). Moreover, *F.*  
620 *albida* improve water infiltration (Diongue et al., 2023; Faye et al., 2020; Sarr et al., 2023), enhance  
621 soil moisture retention (Clermont-Dauphin et al., 2023) and contribute to reduced soil  
622 temperatures (de Carvalho et al., 2021; Lopes et al., 2024; Sida et al., 2018). These changes foster  
623 a more favourable environment for soil microbial activity and crop development (Diack et al.,  
624 2024; Diene et al., 2024; Leroux et al., 2020; Rouspard et al., 2020) under the trees compared to  
625 open areas. Consequently, this likely explains the stronger effect of soil moisture and the leaf area  
626 index of groundnuts on R<sub>ch</sub> under the trees, resulting in higher total respiration (Table 2). For  
627 photosynthesis, the effect of these parameters was similar in both FS and Sh (Table 2). However,  
628 the significantly higher intensity of GPP<sub>ch</sub> under Sh can be explained by greater light use efficiency  
629 ( $\alpha$ ) and a higher maximum CO<sub>2</sub> uptake rate at light saturation ( $\beta$ ) in this shaded environment. In  
630 agroforestry systems, light use efficiency can at least partially mitigate the reduction in  
631 photosynthetically active radiation under tree canopies (Charbonnier et al., 2017).  
632 Similar results have been observed in different climatic conditions and ecosystems. Gomes et al.  
633 (2016) investigated soil respiration using mobile chambers (LI-8100-102 model) under trees in  
634 coffee-based agroforestry (AF) systems and in open areas (FS) in Minas Gerais, Brazil. These  
635 studies were conducted with agroecological management practices, such as weeding,  
636 intercropping maize between coffee rows, and mulching. The AF systems exhibited lower air and  
637 soil temperatures (at 5 and 10 cm depth) and higher air and soil humidity compared to FS (Gomes  
638 et al., 2016). These authors observed greater spatial variability in soil respiration in AF (34.1%)  
639 compared to FS (24.2%). This variability was mainly linked with fluctuations in labile carbon and  
640 total nitrogen, reflecting more favourable soil microclimate for microbial activity in AF. In  
641 contrast, soil temperature (10 cm depth) accounted for most of the variability observed in FS,  
642 where the absence of tree canopy resulted in high soil temperatures and low soil moisture (Gomes  
643 et al., 2016). Likewise, Haren et al. (2010) reported 38% higher soil respiration near large trees  
644 (DBH > 35 cm) in clay-rich Amazonian forests compared to open sites. Interestingly, the  
645 magnitude of CO<sub>2</sub> fluxes was independent of tree species, indicating that canopy effects may  
646 outweigh species-specific traits in some contexts. In our study, *F. albida*'s influence on CO<sub>2</sub> fluxes



647 aligns with this general pattern observed in tropical agroforestry. However, the mechanisms  
648 linking individual tree species to microbial and physicochemical drivers of CO<sub>2</sub> dynamics remain  
649 insufficiently understood and warrant further investigation (Jevon et al., 2023).

#### 650 4.4. Birch Effect

651 A rapid increase in soil respiration was observed following the first rainfall events, particularly  
652 under *F. albida*. This phenomenon can be attributed to the lower bulk density of the soil under the  
653 trees (Clermont-Dauphin et al., 2023; Siegwart et al., 2023), which potentially lead to CO<sub>2</sub>  
654 accumulation during the dry season due to higher soil organic matter (SOM) (Siegwart et al.,  
655 2023). Additionally, the sensitivity of microbial communities to subtle variations in soil moisture,  
656 compounded by the tree effect, may further explain this phenomenon, as outlined in Sections 4.1  
657 and 4.3. This phenomenon, known as the 'Birch effect' (Birch, 1958), has been reported across  
658 various semi-arid ecosystems in sub-Saharan Africa (Ago et al., 2016b; Fan et al., 2015;  
659 Wieckowski et al., 2024), as well as other semi-arid ecosystems globally (Roby et al., 2022; Yan et  
660 al., 2014; Yu et al., 2020). In these contexts, the 'Birch effect' may result from the displacement of  
661 soil gas phases by the piston effect generated during water infiltration (Singh et al., 2023).  
662 Furthermore, microbial communities in semi-arid environments adopt osmoregulatory  
663 mechanisms to withstand water deficit (Warren, 2014), which is particularly pronounced during  
664 the dry season. This phenomenon reduces soil microbial metabolism (Schimel et al., 2007). Upon  
665 rapid soil rewetting, especially after prolonged dry periods, soil microbial metabolism process is  
666 swiftly reactivated, leading to a transient pulse in respiration and a CO<sub>2</sub> release (Barnard et al.,  
667 2020; Kim et al., 2012; Manzoni et al., 2020; Vargas et al., 2018). Isotopic signatures of soil  
668 respiration provide evidence supporting the hypothesis that these pulses result from the rapid  
669 mineralisation of necromass or osmolytes excreted by microorganisms under drought stress  
670 (Schimel et al., 2007; Unger et al., 2010). Additional factors may amplify the 'Birch effect'. For  
671 instance, drying-rewetting cycles can induce physical disruption of soil aggregates, enhance  
672 oxygen penetration and thereby expose previously protected organic matter to microbial  
673 decomposition (Rabbi et al., 2024). This increases substrate availability and subsequently boosts  
674 soil respiration fluxes.

675 The magnitude of the 'Birch effect' is modulated by the severity and duration of drought. Thus, at  
676 our study site, given the 8- to 9-month-long dry season, the 'Birch effect' is particularly intense.  
677 Indeed, extended drought periods promote greater accumulation of microbial necromass and  
678 intensify hypo-osmotic stress responses upon rewetting (Singh et al., 2023).



679 *4.5. Comparing EC and chamber-based methods*

680 Results revealed high seasonal variability, with higher values during the rainy season compared  
681 to the dry season. This seasonal pattern aligns with findings from studies in the Sahel using the  
682 EC method for CO<sub>2</sub> flux measurements (Brümmer et al., 2008; Tagesson et al., 2015; Agbohessou  
683 et al., 2023, Wieckowski et al., 2024). Comparable patterns have been also documented at the  
684 ecosystem scale in other semi-arid environments (Ago et al., 2014; Archibald et al., 2009; Ardö et  
685 al., 2008; Jia et al., 2020; Quansah et al., 2015; Williams et al., 2009; Zhang, Bi, et al., 2024).

686 Several comparative studies between chamber and EC methods have reported both congruent  
687 and divergent CO<sub>2</sub> flux estimates (Bastviken et al., 2022; Poyda et al., 2017; Riederer et al., 2014;  
688 J. Tang et al., 2008; Wang et al., 2010). In the present study, ecosystem respiration fluxes during  
689 the rainy season exhibited notable discrepancies measurements between EC (Reco.EC) and  
690 upscaled chamber-based (Rch.stand). This is attributable to differences in the flux components  
691 captured by each method. Specifically, Reco.EC included respiration from below- and above-  
692 ground tree parts, crops (groundnuts and cowpeas), weeds, and soil, whereas Rch.stand  
693 accounted only respiration from below-ground tree, groundnut crop, and soil. Therefore, as  
694 expected, Reco.EC ( $4.6 \pm 3.2$  g C-CO<sub>2</sub> m<sup>-2</sup> d<sup>-1</sup>) were significantly higher than Rch.stand ( $2.0 \pm 1.1$  g  
695 C-CO<sub>2</sub> m<sup>-2</sup> d<sup>-1</sup>).

696 For chamber-based GPP measurements, values were standardised (GPP-stand) by the field's leaf  
697 area index (LAI.field). This allowed it to improve comparability with GPP.EC when trees were  
698 leafless in the rainy season. In both cases, GPP accounted only for crops (groundnut and cowpea)  
699 and weeds, as trees were non-photosynthetic in the rainy season. Despite this standardisation,  
700 GPP.EC values ( $-5.1 \pm 3.6$  g C-CO<sub>2</sub> m<sup>-2</sup> d<sup>-1</sup>) were significantly higher than GPPch.stand values ( $-4.2$   
701  $\pm 4.3$  g C-CO<sub>2</sub> m<sup>-2</sup> d<sup>-1</sup>). However, the divergence did not occur on the peak of GPP (which was very  
702 similar in both methods), but from the onset of groundnut senescence, when weeds became the  
703 dominant photosynthetic contributors. Thus, during the groundnut growth season, with leafless  
704 *F. albida* trees and almost no weeds, GPP measurements from EC and chambers generate closely  
705 comparable results. Therefore, this provides an initial form of cross-validation between the two  
706 methods. It is important to note that the EC method integrates CO<sub>2</sub> fluxes over a larger spatial  
707 scale, encompassing all ecosystem components (Baldocchi, 2003), while the chamber method  
708 captures fluxes on a smaller scale (i.e., at the 0.25 m<sup>2</sup> scale). This scale disparity can introduce  
709 uncertainties when upscaling chamber-based fluxes to the field, as vegetation composition within  
710 chambers does not represent the EC footprint's average vegetation. This makes upscaling  
711 chamber-based measurements challenging. Nevertheless, the standardisation we applied on  
712 chamber photosynthesis by LAI has been relatively successful.

713 During the dry season, Reco.EC included respiration from below- and above-ground tree parts  
714 (with leaves) and bare soil, while Rch.stand measured only below-ground tree and bare soil



715 respiration. Consequently, the difference between Reco.EC and Rch.stand was solely attributable  
716 to above-ground tree respiration (Ra tree above-ground). In terms of GPP, chamber  
717 measurements were nil, whereas GPP.EC reflected only GPP trees.

718 The transition period, characterised by groundnut senescence, tree leaf regrowth, and weed  
719 proliferation, introduced further complexity, amplifying method-specific discrepancies. Rch.stand  
720 measurements facilitated the estimation of tree contribution to Reco.EC (Ra tree) and the  
721 verification of the consistency for EC results in terms of carbon use efficiency (CUE), estimated  
722 here at 0.48. This value indicates that nearly 50% of the carbon captured by trees is allocated to  
723 biomass. The CUE estimate here is well comparable to the global average across diverse  
724 ecosystems, climates, and management practices ( $0.49 \pm 0.14$ ) (Tang et al., 2019). Similar CUE  
725 values have been reported for semi-arid grasslands ( $0.46 \pm 0.10$ ), but our value is notably lower  
726 than those documented for wetlands ( $0.61 \pm 0.13$ ) (Tang et al., 2019). Overall, these findings  
727 reinforce the plausibility of our assumptions regarding the compartment's contributions to  
728 Reco.EC and Rch.stand, thereby providing a second cross-validation of the EC-Ch comparison.  
729 However, despite a frequently assumed CUE of 0.5 in models, global estimates span a broad range  
730 (0.20 to 0.82), depending on ecosystem type and management practices (DeLucia et al., 2007;  
731 Tang et al., 2019). This underscores the importance of refining carbon flux models to better  
732 represent the biophysical processes governing CO<sub>2</sub> exchange in semi-arid agroforestry systems.  
733 The combined use of EC and chamber methodologies offers a comprehensive perspective on  
734 ecosystem-scale CO<sub>2</sub> flux dynamics, advancing understanding of carbon cycling in these  
735 environments.

#### 736 *4.6. Net carbon exchange budget*

737 The annual net carbon (C) exchange budget was quantified at  $-1.4 \pm 0.02$  Mg C-CO<sub>2</sub> ha<sup>-1</sup> with the  
738 chamber method and  $-1.8 \pm 0.01$  Mg C-CO<sub>2</sub> ha<sup>-1</sup> by the Eddy Covariance (EC), indicating that the  
739 studied agro-silvo-pastoral system functions as a net carbon sink. These findings corroborate the  
740 system's potential role in mitigating greenhouse gas emissions, consistent with previous  
741 observations in semi-arid ecosystems (Rahimi et al., 2021; Tagesson et al., 2015; Agbohessou et  
742 al., 2023, Wieckowski et al., 2024).

743 The estimated net C exchange budget is close to the reported mean for Sahelian ecosystems ( $-1.6$   
744  $\pm 0.5$  Mg C-CO<sub>2</sub> ha<sup>-1</sup>; Tagesson et al., 2016). The EC-based net C exchange budget ( $-1.8 \pm 0.01$  Mg  
745 C-CO<sub>2</sub> ha<sup>-1</sup>) is also similar to the value of  $-1.9 \pm 0.4$  Mg C-CO<sub>2</sub> ha<sup>-1</sup> reported for semi-arid savannas  
746 of northeastern Benin, despite higher annual rainfall (1495 mm; Ago et al., 2016b). Furthermore,  
747 our EC estimate is close to the average net C exchange reported for West African terrestrial  
748 ecosystems ( $-2.0 \pm 1.5$  Mg C-CO<sub>2</sub> ha<sup>-1</sup>; Ago et al., 2016a).



749 However, estimates from Tagesson et al. (2015) ( $-2.7 \pm 0.07$  Mg C-CO<sub>2</sub> ha<sup>-1</sup>) for a semi-arid  
750 savannah in Dahra, Senegal, located between the 300 mm and 400 mm isohyets, were  
751 comparatively higher. This is potentially attributable to specific characteristics of that specific  
752 savannah site, such as herbaceous vegetation cover during the rainy season, the presence of  
753 evergreen trees, and land management practices linked to pastoral livestock activities (Tagesson  
754 et al., 2016).

755 The net C exchange estimates presented in this study are, in fact, apparent fluxes, given that they  
756 exclude organic matter (OM) imports and, more critically, exports, introducing uncertainties.  
757 Notably, the export of crop residues and direct inputs from animal excreta —particularly  
758 significant in ‘bush fields’ during the dry season — were not accounted for. In our case of ‘bush  
759 field’, crop residues are exported to feed livestock, while livestock faeces are collected for use as  
760 fuel or manure in ‘home fields’. Such practices may lead to a significant soil organic carbon stocks  
761 depletion (Malou et al, 2021), potentially diminishing the net C budget ( $-1.4 \pm 0.02$  Mg C-CO<sub>2</sub> ha<sup>-1</sup>)  
762 over time and shifting the system closer to carbon neutrality (Assouma et al., 2019).

763 These results should be contextualized within the broader framework of climate change and semi-  
764 arid ecosystem management. Although agro-silvo-pastoral systems can function as annual carbon  
765 sinks, they remain highly sensitive to interannual rainfall variability and escalating anthropogenic  
766 pressures. Sustainable management practices, particularly regarding crop residue exports, are  
767 essential for maintaining soil mineral fertility and preserving the system’s capacity to act as a  
768 carbon sink, thereby contributing to climate change mitigation.

#### 769 *4.7. Limitations of the study*

770 This study benefited from the inverse phenology of *F. albida*, allowing for direct comparison  
771 between chamber-based GPP (GPPch.stand) and ecosystem-level GPP (GPP.EC) during the  
772 leafless period of the trees. However, the system’s spatial heterogeneity —common in  
773 agroforestry— posed challenges for accurately partitioning CO<sub>2</sub> fluxes among trees, crops, and  
774 soil. A key limitation was the development of weeds during the late rainy season, which  
775 complicated the attribution of fluxes, particularly during the transitional period. Additionally,  
776 while GPPch was successfully standardised by LAI for upscaling, this was not feasible for  
777 respiration. Respiration integrates both autotrophic and heterotrophic components, which  
778 respond to different drivers and are not directly linked to LAI, limiting the precision of upscaled  
779 Rch.

780 Future improvements should aim to separately quantify respiration sources —tree roots, crops,  
781 and microbial (heterotrophic) respiration— and account explicitly for the weed layer, to refine  
782 flux partitioning in such complex agroforestry systems.



783 **Conclusion**

784 This study demonstrates the successful application of automated static chambers to quantify CO<sub>2</sub>  
785 fluxes in a Sahelian agroforestry system dominated by *F. albida*. The continuous, high-frequency  
786 measurements captured key seasonal dynamics and short-lived events (e.g., Birch effect),  
787 providing a more accurate assessment of carbon exchange than traditional intermittent sampling.  
788 By integrating crop and soil components and applying dynamic partitioning models, the study  
789 quantified both respiration and photosynthesis fluxes at fine temporal resolution. The results  
790 revealed a clear 'fertile island' effect under tree canopies, with higher respiration and  
791 photosynthetic activity, and highlighted the significant contribution of *F. albida* trees to annual  
792 carbon uptake.

793 The consistency between chamber- and eddy covariance-based estimates reinforces the  
794 robustness of the methodology. Overall, this work underscores the role of *F. albida*-based  
795 agroforestry systems as effective carbon sinks in semi-arid environments, offering valuable  
796 insights for carbon accounting and sustainable land management in the Sahel.



797 **Acknowledgments**

798 This research was financially supported by the CaSSECS project (Carbon Sequestration and  
799 Greenhouse Gas Emissions in (Agro) Silvopastoral Systems of the CILS-Sahel States  
800 (FOOD/2019/410-169), within the framework of the European Union's initiative 'Development  
801 of Smart Innovation through Agricultural Research' (DeSIRA-UE-EuropAID). We extend our  
802 sincere gratitude to the coordination team of the CaSSECS project, the "Laboratoire Mixte  
803 International Intensification Écologique des Sols Cultivés en Afrique de l'Ouest" (LMI IESOL) of  
804 the of the French National Institute for Development (IRD) in Dakar (Senegal), as well as to the  
805 Faidherbia-Flux platform (<https://lped.info/wikiObsSN/?Faidherbia-Flux>), its partners, and  
806 affiliated projects PEPR FairCarbonN/PC3-RIFT, EU-H2020 |SUSTAIN-SAHEL (Grant N° 861974)]  
807 and EU-HORIZON EUROPE [GALILEO (Grant N° 101181623) ]. Our deepest appreciation goes to  
808 Ibou Diouf, the observer at our experimental site. Tagesson also acknowledged funding from  
809 Formas (Dnr 2021-00644).



810 **Author contribution: CRediT**

811 **Seydina Mohamad BA:** Conducting in situ experiments, collecting and processing data,  
812 writing-original draft, review and editing. **Olivier Roupsard:** Designing experimental  
813 apparatus and methodology, writing, review and editing. **Lydie Chapuis-Lardy:** Designing  
814 methodology, writing, review and editing. **Yélognissè Agbohessou:** Processing data,  
815 review and editing. **Fred Bouvery:** Designing chambers and connection to the instrument,  
816 review and editing. **Maxime Duthoit:** Designing experimental set and methodology,  
817 review and editing. **Aleksander Wieckowski:** Review and editing. **Mohamed Habibou**  
818 **Assouma:** Review and editing. **Espoir Gaglo:** Processing data, review and editing. **Claire**  
819 **Delon:** review and editing. **Torbern Tagesson:** Designing methodology, review, and  
820 editing. **Bienvenu Sambou:** Review and editing. **Dominique Serça:** Designing methodology,  
821 writing, review and editing.



822 **References**

823 Agbohessou, Y., Delon, C., Mougin, E., Grippa, M., Tagesson, T., Diedhiou, M., Ba, S., Ngom, D., Vezy,  
824 R., Ndiaye, O., Assouma, M. H., Diawara, M., & Rouspard, O.: To what extent are greenhouse-gas  
825 emissions offset by trees in a Sahelian silvopastoral system?, *Agr. Forest. Meteorol.*, 343, 109780,  
826 <https://doi.org/10.1016/j.agrformet.2023.109780>, 2023.

827 Agbohessou, Y., Delon, C., Grippa, M., Mougin, E., Ngom, D., Gaglo, E. K., Ndiaye, O., Salgado, P., and  
828 Rouspard, O.: Modelling CO<sub>2</sub> and N<sub>2</sub>O emissions from soils in silvopastoral systems of the West  
829 African Sahelian band. *Biogeosciences*, 21, 2811–2837, [https://doi.org/10.5194/bg-21-2811-](https://doi.org/10.5194/bg-21-2811-2024)  
830 [2024](https://doi.org/10.5194/bg-21-2811-2024), 2024.

831 Ago, E., Agbossou, K., Ozer, P., & Aubinet, M.: Mesure des flux de CO<sub>2</sub> et séquestration de carbone  
832 dans les écosystèmes terrestres ouest-africains (synthèse bibliographique), *Biotechnologie,*  
833 *Biotechnol. Agron. Soc. Environ.*, 20(1), 68-82, <https://doi.org/10.25518/1780-4507.12565>,  
834 2016a.

835 Ago, E., Agbossou, E. K., Cohard, J. M., Galle, S., & Aubinet, M.: Response of CO<sub>2</sub> fluxes and  
836 productivity to water availability in two contrasting ecosystems in northern Benin (West Africa),  
837 *Ann. Forest. Sci.*, 73(2), 483-500, <https://doi.org/10.1007/s13595-016-0542-9>, 2016b.

838 Ago, E., Agbossou, E. K., Galle, S., Cohard, J. M., Heinesch, B., & Aubinet, M.: Long term observations  
839 of carbon dioxide exchange over cultivated savanna under a Sudanian climate in Benin (West  
840 Africa), *Agr. Forest. Meteorol.*, 197, 13-25, <https://doi.org/10.1016/j.agrformet.2014.06.005>,  
841 2014.

842 Archibald, S. A., Kirton, A., van der Merwe, M.R, Scholes, R. J., Williams, C.A, & Hanan, H.: Drivers of  
843 inter-annual variability in Net Ecosystem Exchange in a semi-arid savanna ecosystem, South  
844 Africa, *Biogeosciences*, 6, 251–266, <https://doi.org/10.5194/bg-6-251-2009>, 2009.

845 Ardö, J., Mölder, M., El-Tahir, B. A., & Elkhidir, H. A. M.: Seasonal variation of carbon fluxes in a  
846 sparse savanna in semi-arid Sudan, *Carbon Balance and Management*, 3(1), 7,  
847 <https://doi.org/10.1186/1750-0680-3-7>, 2008.

848 Assefa, A., Muthuri, C. W., Gebrekirstos, A., Hadgu, K., & Fetene, M.: Tree growth and wheat  
849 productivity are affected by pollarding *Faidherbia albida* in semi-arid Ethiopia, *Agroforest. Syst.*,  
850 98(3), 783-796, <https://doi.org/10.1007/s10457-023-00948-7>, 2024.



- 851 Assouma, M. H., Hiernaux, P., Lecomte, P., Ickowicz, A., Bernoux, M., & Vayssières, J.: Contrasted  
852 seasonal balances in a Sahelian pastoral ecosystem result in a neutral annual carbon balance,  
853 *Journal of Arid Environments*, 162, 62-73, <https://doi.org/10.1016/j.jaridenv.2018.11.013>, 2019.
- 854 Assouma, M. H., Serça, D., Guérin, F., Blanfort, V., Lecomte, P., Touré, I., Ickowicz, A., Manlay, R. J.,  
855 Bernoux, M., & Vayssières, J.: Livestock induces strong spatial heterogeneity of soil CO<sub>2</sub>, N<sub>2</sub>O and  
856 CH<sub>4</sub> emissions within a semi-arid sylvo-pastoral landscape in West Africa, *Journal of Arid Land*,  
857 9(2), 210-221, <https://doi.org/10.1007/s40333-017-0001-y>, 2017.
- 858 Bado, B. V., Whitbread, A., & Sanoussi Manzo, M. L.: Improving agricultural productivity using  
859 agroforestry systems: Performance of millet, cowpea, and ziziphus-based cropping systems in  
860 West Africa Sahel, *Agr. Ecosyst. Environ.*, 305, 107175,  
861 <https://doi.org/10.1016/j.agee.2020.107175>, 2021.
- 862 Bahn, M., Reichstein, M., Davidson, E. A., Grünzweig, J., Jung, M., Carbone, M. S., Epron, D., Misson,  
863 L., Nouvellon, Y., Rouspard, O., Savage, K., Trumbore, S. E., Gimeno, C., Curiel Yuste, J., Tang, J.,  
864 Vargas, R., & Janssens, I. A.: Soil respiration at mean annual temperature predicts annual total  
865 across vegetation types and biomes, *Biogeosciences*, 7(7), 2147-2157,  
866 <https://doi.org/10.5194/bg-7-2147-2010>, 2010.
- 867 Baldocchi, D.: Assessing the eddy covariance technique for evaluating carbon dioxide exchange  
868 rates of ecosystems: Past, present and future, *Glob. Change Biol.*, 9, 479-492,  
869 <https://doi.org/10.1046/j.1365-2486.2003.00629.x>, 2003.
- 870 Baldocchi, D.: « Breathing » of the terrestrial biosphere: Lessons learned from a global network of  
871 carbon dioxide flux measurement systems, *Aust. J. Bot.*, 56(1), 1,  
872 <https://doi.org/10.1071/BT07151>, 2008.
- 873 Baldocchi, D.: How eddy covariance flux measurements have contributed to our understanding of  
874 global change biology, *Glob. Change Biol.*, 26: 242-260, <https://doi.org/10.1111/gcb.14807>,  
875 2020.
- 876 Barnard, R. L., Blazewicz, S. J., & Firestone, M. K.: Rewetting of soil: Revisiting the origin of soil CO<sub>2</sub>  
877 emissions, *Soil Biology and Biochemistry*, 147, <https://doi.org/10.1016/j.soilbio.2020.107819>,  
878 2020.
- 879 Bastviken, D., Wilk, J., Duc, N. T., Gålfalk, M., Karlson, M., Neset, T.-S., Opach, T., Enrich-Prast, A., &  
880 Sundgren, I.: Critical method needs in measuring greenhouse gas fluxes. *Environmental Research*  
881 *Letters*, 17(10), 104009, <https://doi.org/10.1088/1748-9326/ac8fa9>, 2022.



- 882 Bayala, J., Sanou, J., Bazié, H. R., Coe, R., Kalinganire, A., & Sinclair, F. L.: Regenerated trees in  
883 farmers' fields increase soil carbon across the Sahel, *Agroforest. Syst.*, 94(2), 401-415,  
884 <https://doi.org/10.1007/s10457-019-00403-6>, 2020.
- 885 Birch, H. F.: The effect of soil drying on humus decomposition and nitrogen availability, *Plant and*  
886 *Soil*, 10(1), 9-31, <https://doi.org/10.1007/BF01343734>, 1958.
- 887 Bombelli A, Henry M., Castaldi S., Adu-Bredu S, Arneth A, De Grandcourt A, Grieco E., Kutsch  
888 W.L., Lehsten V., Rasile A., Reichstein M, Tansey K., Weber U, Valentini R.: An outlook on the Sub-  
889 Saharan Africa carbon balance, *Biogeosciences*, 6 (10), 2193-2205, [https://doi.org/10.5194/bg-](https://doi.org/10.5194/bg-6-2193-2009)  
890 [6-2193-2009](https://doi.org/10.5194/bg-6-2193-2009), 2009.
- 891 Borken, W., Xu, Y., Davidson, E. A., & Beese, F.: Site and temporal variation of soil respiration in  
892 European beech, Norway spruce, and Scots pine forests, *Glob. Change Biol.*, 8(12), 1205-1216,  
893 <https://doi.org/10.1046/j.1365-2486.2002.00547.x>, 2002.
- 894 Bréchet, L. M., Daniel, W., Stahl, C., Burban, B., Goret, J. Y., Salomón, R. L., & Janssens, I. A.:  
895 Simultaneous tree stem and soil greenhouse gas (CO<sub>2</sub>, CH<sub>4</sub>, N<sub>2</sub>O) flux measurements: A novel  
896 design for continuous monitoring towards improving flux estimates and temporal resolution, *New*  
897 *Phytologist*, 230(6), 2487-2500, <https://doi.org/10.1111/nph.17352>, 2021.
- 898 Bréchet, L. M., Salomón, R. L., Machacova, K., Stahl, C., Burban, B., Goret, J. Y., Steppe, K., Damien, B.,  
899 & Janssens, I. A.: Insights into the sub daily variations in methane, nitrous oxide and carbon  
900 dioxide fluxes from upland tropical tree stems, *New Phytologist*, 20401,  
901 <https://doi.org/10.1111/nph.20401>, 2025.
- 902 Brümmer, C., Falk, U., Papen, H., Szarzynski, J., Wassmann, R., & Brüggemann, N.: Diurnal, seasonal,  
903 and interannual variation in carbon dioxide and energy exchange in shrub savanna in Burkina  
904 Faso (West Africa), *Biogeosciences*, 113, G2030, <https://doi.org/10.1029/2007JG000583>, 2008.
- 905 Brümmer, C., Papen, H., Wassmann, R., & Brüggemann, N.: Fluxes of CH<sub>4</sub> and CO<sub>2</sub> from soil and  
906 termite mounds in south Sudanian savanna of Burkina Faso (West Africa), *Global Biogeochemical*  
907 *Cycles*, 23, GB1001, <https://doi.org/10.1029/2008GB003237>, 2009.
- 908 Cardinael, R., Cadisch, G., Gosme, M., Oelbermann, M., & Van Noordwijk, M.: Climate change  
909 mitigation and adaptation in agriculture: Why agroforestry should be part of the solution? *Agr.*  
910 *Ecosyst. Environ.*, 319, 107555, <https://doi.org/10.1016/j.agee.2021.107555>, 2021.



- 911 Charbonnier, F., Roupsard, O., le Maire, G., Guillemot, J., Casanoves, F., Lacoite, A., Vaast, P.,  
912 Allinne, C., Audebert, L., Cambou, A., Clément-Vidal, A., Defrenet, E., Duursma, R. A., Jarri, L.,  
913 Jourdan, C., Khac, E., Leandro, P., Medlyn, B. E., Saint-André, L., Thaler, P., Van Den Meersche, K.,  
914 Barquero Aguilar, A., Lehner, P., & Dreyer, E.: Increased light-use efficiency sustains net primary  
915 productivity of shaded coffee plants in agroforestry system, *Plant Cell and Environment*, 40(8),  
916 1592-1608, <https://doi.org/10.1111/pce.12964>, 2017.
- 917 Chu, H., Luo, X., Ouyang, Z., et al.: Representativeness of Eddy-Covariance flux footprints for areas  
918 surrounding AmeriFlux sites, *Agr. Forest. Meteorol.*, 301-302, 108350,  
919 <https://doi.org/10.1016/j.agrformet.2021.108350>, 2021.
- 920 Clermont-Dauphin, C., N'dienor, M., Leroux, L., Ba, Halimatou. S., Bongers, F., Jourdan, C., Roupsard,  
921 O., Do, F. C., Cournac, L., & Seghier, J.: *Faidherbia albida* trees form a natural buffer against millet  
922 water stress in agroforestry parklands in Senegal, *Biotechnol. Agron. Soc. Environ*, 182-195,  
923 <https://doi.org/10.25518/1780-4507.20477>, 2023.
- 924 Conant, R. T., Dalla-Betta, P., Klopatek, C. C., & Klopatek, J. M.: Controls on soil respiration in  
925 semiarid soils, *Soil Biology and Biochemistry*, 36(6), 945-951,  
926 <https://doi.org/10.1016/j.soilbio.2004.02.013>, 2004.
- 927 Crosson, E.: A cavity ring-down analyzer for measuring atmospheric levels of methane, carbon  
928 dioxide, and water vapor, *App. Phys. B-Lasers O.*, 92, 403-408, [https://doi.org/10.1007/s00340-](https://doi.org/10.1007/s00340-008-3135-y)  
929 [008-3135-y](https://doi.org/10.1007/s00340-008-3135-y), 2008.
- 930 de Carvalho, A. F., Fernandes-Filho, E. I., Daher, M., Gomes, L. de C., Cardoso, I. M., Fernandes, R. B.  
931 A., & Schaefer, C. E. G. R.: Microclimate and soil and water loss in shaded and unshaded  
932 agroforestry coffee systems, *Agroforest. Syst.*, 95(1), 119-134, [https://doi.org/10.1007/s10457-](https://doi.org/10.1007/s10457-020-00567-6)  
933 [020-00567-6](https://doi.org/10.1007/s10457-020-00567-6), 2021.
- 934 Delon, C., Galy-Lacaux, C., Serça, D., Personne, E., Mouglin, E., Adon, M., ... & Tagesson, T.: Modelling  
935 land-atmosphere daily exchanges of NO, NH<sub>3</sub>, and CO<sub>2</sub> in a semi-arid grazed ecosystem in Senegal,  
936 *Biogeosciences*, 16(9), 2049-2077, <https://doi.org/10.5194/bg-16-2049-2019>, 2019.
- 937 Delaunay, V., Desclaux, A., & Sokhna, Ch.: *Niakhar, mémoires et perspectives: Recherches*  
938 *pluridisciplinaires sur le changement en Afrique*, IRD Éditions/L'Harmattan, 536 p., ISBN  
939 9782140103551, 2140103556 [https://www.editions.ird.fr/open\\_access\\_download/851/441](https://www.editions.ird.fr/open_access_download/851/441),  
940 2019.



- 941 DeLucia, E. H., Drake, J. E., Thomas, R. B., & Gonzalez-Meler, M.: Forest carbon use efficiency: Is  
942 respiration a constant fraction of gross primary production?, *Glob. Change Biol.*, 13(6),  
943 1157-1167, <https://doi.org/10.1111/j.1365-2486.2007.01365.x>, 2007.
- 944 Denmead, O. T.: Approaches to measuring fluxes of methane and nitrous oxide between  
945 landscapes and the atmosphere, *Plant and Soil*, 309(1-2), 5-24, [https://doi.org/10.1007/s11104-  
946 008-9599-z](https://doi.org/10.1007/s11104-008-9599-z), 2008.
- 947 Diack, I., Diene, S., Leroux, L., Diouf, A., Benjamin, H., Olivier, R., Letourmy, P., Alain, A., Sarr, I., &  
948 Moussa, D.: Combining UAV and Sentinel-2 Imagery for Estimating Millet FCover in a  
949 Heterogeneous Agricultural Landscape of Senegal, *IEEE Journal of Selected Topics in Applied  
950 Earth Observations and Remote Sensing*, 17, 7305-7322,  
951 <https://doi.org/10.1109/JSTARS.2024.3373508>, 2024.
- 952 Diene, S. M., Diack, I., Audebert, A., Roupsard, O., Leroux, L., Diouf, A. A., Mbaye, M., Fernandez, R.,  
953 Diallo, M., Sarr, I.: Improving pearl millet yield estimation from UAV imagery in the semiarid  
954 agroforestry system of Senegal through textural indices and reflectance normalization, in *IEEE  
955 Access*, 12, 132626-132643, <https://doi.org/10.1109/ACCESS.2024.3460107>, 2024.
- 956 Dilla, A. M., Smethurst, P. J., Barry, K., & Parsons, D.: Preliminary estimate of carbon sequestration  
957 potential of *Faidherbia albida* (Delile) A. Chev in an agroforestry parkland in the Central Rift Valley  
958 of Ethiopia, *Forests, Trees and Livelihoods*, 28(2), 79-89,  
959 <https://doi.org/10.1080/14728028.2018.1564146>, 2019.
- 960 Diongue, D., Brunetti, G., Stumpp, C., Do, F., Roupsard, O., Orange, D., Faye, W., Sow, S., Jourdan, C.,  
961 & Faye, S.: A Probabilistic Framework for Assessing the Hydrological Impact of *Faidherbia Albida*  
962 in an Arid Area of Senegal, *Journal of Hydrology*, 622, 129717,  
963 <https://doi.org/10.1016/j.jhydrol.2023.129717>, 2023.
- 964 Diongue, D. M. L., Roupsard, O., Do, F. C., Stumpp, C., Orange, D., Sow, S., Jourdan, C., & Faye, S.:  
965 Evaluation of parameterisation approaches for estimating soil hydraulic parameters with  
966 HYDRUS-1D in the groundnut basin of Senegal, *Hydrological Sciences Journal*, 67(15), 2327-  
967 2343, <https://doi.org/10.1080/02626667.2022.2142474>, 2022.
- 968 Duthoit, M., Roupsard, O., Créquy, N., & Sauze, J.: Conception d'un dispositif automatisé de  
969 chambres de mesures d'échanges gazeux du sol à fermeture horizontale, *Le Cahier des Techniques  
970 de l'Inra*, 102, 19 p., hal-03989886, <https://hal.science/hal-03989886/document>, 2020.



- 971 Eldridge, D.J., Ding, J., Dorrough, J. et al. Hotspots of biogeochemical activity linked to aridity and  
972 plant traits across global drylands. *Nat. Plants* 10, 760–770 (2024).  
973 <https://doi.org/10.1038/s41477-024-01670-7>
- 974 Evans, S., Dieckmann, U., Franklin, O., & Kaiser, C.: Synergistic effects of diffusion and microbial  
975 physiology reproduce the Birch effect in a micro-scale model, *Soil Biology and Biochemistry*, 93,  
976 28-37, <https://doi.org/10.1016/j.soilbio.2015.10.020>, 2016.
- 977 Falge, E., Baldocchi, D., Olson, R., Anthoni, P., Aubinet, M., Bernhofer, C., Burba, G., Ceulemans, R.,  
978 Clement, R., Dolman, H., Granier, A., Gross, P., Grünwald, T., Hollinger, D., Jensen, N.-O., Katul, G.,  
979 Keronen, P., Kowalski, A., Ta Lai, C., ... Oren, R.: Gap filling strategies for defensible annual sums of  
980 net ecosystem exchange, *Agr. Forest Meteorol.*, 107, 43-69, [https://doi.org/10.1016/S0168-](https://doi.org/10.1016/S0168-1923(00)00225-2)  
981 [1923\(00\)00225-2](https://doi.org/10.1016/S0168-1923(00)00225-2), 2001.
- 982 Fan, Z., Neff, J. C., & Hanan, N. P.: Modeling pulsed soil respiration in an African savanna ecosystem,  
983 *Agr. Forest Meteorol.*, 200, 282-292, <https://doi.org/10.1016/j.agrformet.2014.10.009>, 2015.
- 984 Fang, F., Han, X., Liu, W., & Tang, M.: Carbon dioxide fluxes in a farmland ecosystem of the southern  
985 Chinese Loess Plateau measured using a chamber-based method, *PeerJ*, 8, 8994,  
986 <https://doi.org/10.7717/peerj.8994>, 2020.
- 987 Faye, W., Fall, A. N., Orange, D., Do, F., Roupsard, O., & Kane, A.: Climatic variability in the Sine-  
988 Saloum basin and its impacts on water resources: Case of the Sob and Diahine watersheds in the  
989 region of Niakhar, *Proceedings of the International Association of Hydrological Sciences*, 383,  
990 391-399, <https://doi.org/10.5194/piahs-383-391-2020>, 2020.
- 991 Finkelstein, P. L., & Sims, P. F.: Sampling error in eddy correlation flux measurements, *J. Geophys.*  
992 *Res.*, 106(D4), 3503–3509, <https://doi.org/10.1029/2000JD900731>, 2001.
- 993 Fleck, D., He, Y., Alexander, C., Jacobson, G., & Cunningham, K. L.: Simultaneous soil flux  
994 measurements of five gases-N<sub>2</sub>O, CH<sub>4</sub>, CO<sub>2</sub>, NH<sub>3</sub>, and H<sub>2</sub>O-with the Picarro G2508," Picarro  
995 Application Note, AN034,  
996 [https://www.picarro.com/sites/default/files/product\\_documents/Picarro AN034 Soil%20Flux](https://www.picarro.com/sites/default/files/product_documents/Picarro_AN034_Soil%20Flux%20with%20the%20G2508_1.pdf)  
997 [%20with%20the%20G2508\\_1.pdf](https://www.picarro.com/sites/default/files/product_documents/Picarro_AN034_Soil%20Flux%20with%20the%20G2508_1.pdf), 2013.
- 998 Foken, T., Göockede, M., Mauder, M., Mahrt, L., Amiro, B., Munger, W.: Post-Field Data Quality  
999 Control, In: Lee, X., Massman, W., Law, B. (eds) *Handbook of Micrometeorology*, *Atmos. Ocean. Sci.*  
1000 *Lib.*, vol 29, Springer, Dordrecht, [https://doi.org/10.1007/1-4020-2265-4\\_9](https://doi.org/10.1007/1-4020-2265-4_9), 2004.



- 1001 Foken, T., Aubinet, M., & Leuning, R.: Eddy Covariance. In M. Aubinet, T. Vesala, & D. Papale (eds),  
1002 Eddy Covariance, p.1-19, Springer, Netherlands, <https://doi.org/10.1007/978-94-007-2351-1>,  
1003 2012.
- 1004 Fox, J., Weisberg, S., & Price, B.: car: Companion to Applied Regression (version 3.1-3) [Dataset].  
1005 <https://doi.org/10.32614/CRAN.package.car>, 2023.
- 1006 Gomes, L. D. C., Cardoso, I. M., Mendonça, E. D. S., Fernandes, R. B. A., Lopes, V. S., & Oliveira, T. S.:  
1007 Trees modify the dynamics of soil CO<sub>2</sub> efflux in coffee agroforestry systems, *Agr. Forest. Meteorol.*,  
1008 224, 30-39, <https://doi.org/10.1016/j.agrformet.2016.05.001>, 2016.
- 1009 Gonsamo, A., Chen, J. M., He, L., Sun, Y., Rogers, C., & Liu, J.: Exploring SMAP and OCO-2 observations  
1010 to monitor soil moisture control on photosynthetic activity of global drylands and croplands,  
1011 *Remote Sensing of Environment*, 232, 111314, <https://doi.org/10.1016/j.rse.2019.111314>, 2019.
- 1012 Guillen-Cruz, G., Campuzano, E. F., Juárez-Altamirano, R., López-García, K. L., Torres-Arreola, R., &  
1013 Flores-Rentería, D.: Interannual Variation and Control Factors of Soil Respiration in Xeric  
1014 Shrubland and Agricultural Sites from the Chihuahuan Desert, Mexico, *Land*, 12(11), 1961,  
1015 <https://doi.org/10.3390/land12111961>, 2023.
- 1016 Gupta, S.R., Dagar, J.C., Sileshi, G.W., Chaturvedi, R.K.: Agroforestry for Climate Change Resilience  
1017 in Degraded Landscapes. In: Dagar, J.C., Gupta, S.R., Sileshi, G.W. (eds) *Agroforestry for Sustainable*  
1018 *Intensification of Agriculture in Asia and Africa*, Sustainability Sciences in Asia and Africa,  
1019 Springer, Singapore. [https://doi.org/10.1007/978-981-19-4602-8\\_5](https://doi.org/10.1007/978-981-19-4602-8_5), 2023.
- 1020 Houghton, R. A. and Hackler, J. L.: Emissions of carbon from land use change in sub-Saharan Africa,  
1021 *Geophys. Res.*, 111, G02003, <https://doi.org/10.1029/2005JG000076>, 2006.
- 1022 IUSS Working Group WRB.: World Reference Base for Soil Resources. International soil  
1023 classification system for naming soils and creating legends for soil maps, 4th edition, International  
1024 Union of Soil Sciences (IUSS), Vienna, Austria, ISBN 979-8-9862451-1-9,  
1025 [www.isric.org/sites/default/files/WRB\\_fourth\\_edition\\_2022-12-18.pdf](http://www.isric.org/sites/default/files/WRB_fourth_edition_2022-12-18.pdf), 2022.
- 1026 Jackson, R.B., Canadell, J., Ehleringer, J.R. et al.: A global analysis of root distributions for terrestrial  
1027 biomes, *Oecologia* 108, 389–411, <https://doi.org/10.1007/BF00333714>, 1996.
- 1028 Jevon, F. V., Gewirtzman, J., Lang, A. K., Ayres, M. P., & Matthes, J. H.: Tree Species Effects on Soil  
1029 CO<sub>2</sub> and CH<sub>4</sub> Fluxes in a Mixed Temperate Forest, *Ecosystems*, 26(7), 1587-1602,  
1030 <https://doi.org/10.1007/s10021-023-00852-2>, 2023.



- 1031 Jia, X., Mu, Y., Zha, T., Wang, B., Qin, S., & Tian, Y.: Seasonal and interannual variations in ecosystem  
1032 respiration in relation to temperature, moisture, and productivity in a temperate semi-arid  
1033 shrubland, *Science of The Total Environment*, 709, 136210,  
1034 <https://doi.org/10.1016/j.scitotenv.2019.136210>, 2020.
- 1035 Kim, D. G., Vargas, R., Bond-Lamberty, B., & Turetsky, M. R.: Effects of soil rewetting and thawing  
1036 on soil gas fluxes: A review of current literature and suggestions for future research,  
1037 *Biogeosciences*, 9(7), 2459-2483, <https://doi.org/10.5194/bg-9-2459-2012>, 2012.
- 1038 Kim, D.-G., Thomas, A. D., Pelster, D., Rosenstock, T. S., & Sanz-Cobena, A.: Greenhouse gas  
1039 emissions from natural ecosystems and agricultural lands in sub-Saharan Africa: Synthesis of  
1040 available data and suggestions for further research, *Biogeosciences*, 13(16), 4789-4809,  
1041 <https://doi.org/10.5194/bg-13-4789-2016>, 2016.
- 1042 Klaus, M., Öquist, M., & Macháčová, K.: Tree stem-atmosphere greenhouse gas fluxes in a boreal  
1043 riparian forest, *Science of The Total Environment*, 954, 176243,  
1044 <https://doi.org/10.1016/j.scitotenv.2024.176243>, 2024.
- 1045 Kormann, R., & Meixner, F. X.: An analytical footprint model for non-neutral stratification,  
1046 *Boundary-Layer Meteorology*, 99, 207-224, <https://doi.org/10.1023/A:1018991015119>, 2001.
- 1047 Kuyah, S., Whitney, C. W., Jonsson, M., Sileshi, G. W., Öborn, I., Muthuri, C. W., & Luedeling, E.:  
1048 Agroforestry delivers a win-win solution for ecosystem services in sub-Saharan Africa. A meta-  
1049 analysis, *Agronomy for Sustainable Development*, 39(5), [https://doi.org/10.1007/s13593-019-](https://doi.org/10.1007/s13593-019-0589-8)  
1050 [0589-8](https://doi.org/10.1007/s13593-019-0589-8), 2019.
- 1051 Lambers, H., Chapin, F. S., & Pons, T. L.: *Plant Physiological Ecology*, Springer New York.  
1052 <https://doi.org/10.1007/978-0-387-78341-3>, 2008.
- 1053 Lasslop, G., Reichstein, M., Papale, D., Richardson, A., Arneeth, A., Barr, A., Stoy, P., & Wohlfahrt, G.:  
1054 Separation of net ecosystem exchange into assimilation and respiration using a light response  
1055 curve approach: Critical issues and global evaluation, *Glob. Change Biol.*, 16(1), 187-208.  
1056 <https://doi.org/10.1111/j.1365-2486.2009.02041.x>, 2010.
- 1057 Lembrechts J.J., Aalto J, Ashcroft MB, et al.: SoilTemp: A global database of near-surface  
1058 temperature, *Glob. Change Biol.*, 26, 6616–6629, <https://doi.org/10.1111/gcb.15123>, 2020.
- 1059 Lembrechts, J. J., van den Hoogen, J., Aalto, J., et al.: Global maps of soil temperature. *Glob. Change*  
1060 *Biol.*, 28, 3110-3144, <https://doi.org/10.1111/gcb.16060>, 2022.



- 1061 Leroux, L., Falconnier, G. N., Diouf, A. A., Ndao, B., Gbodjo, J. E., Tall, L., Balde, A. A., Clermont-  
1062 Dauphin, C., Bégué, A., Affholder, F., & Rouspard, O.: Using remote sensing to assess the effect of  
1063 trees on millet yield in complex parklands of Central Senegal, *Agr. Syst.*, 184,  
1064 <https://doi.org/10.1016/j.agry.2020.102918>, 2020.
- 1065 Liu, W., Zhang, Z., & Wan, S.: Predominant role of water in regulating soil and microbial respiration  
1066 and their responses to climate change in a semiarid grassland, *Glob. Change Biol.*, 15(1), 184-195,  
1067 <https://doi.org/10.1111/j.1365-2486.2008.01728.x>, 2009.
- 1068 Liu, Y., He, N., Wen, X., Xu, L., Sun, X., Yu, G., Liang, L., & Schipper, L. A.: The optimum temperature  
1069 of soil microbial respiration: Patterns and controls, *Soil Biology and Biochemistry*, 121, 35-42,  
1070 <https://doi.org/10.1016/j.soilbio.2018.02.019>, 2018.
- 1071 Lloyd, J., & Taylor, J. A.: On the Temperature Dependence of Soil Respiration, *Functional Ecology*,  
1072 8(3), 315-323, <https://doi.org/10.2307/2389824>, 1994.
- 1073 Lopes, V. S., Cardoso, I. M., Cavalcante, V. S., Gomes, L. de C., Tanure, M. M. C., Moura, W. de M.,  
1074 Mendonça, E. de S., & Fernandes, R. B. A.: Soil CO<sub>2</sub> efflux in coffee agroforestry and full-sun coffee  
1075 systems, *Acta Sci. – Agr.*, 46(1), e65877, <https://doi.org/10.4025/actasciagron.v46i1.65877>,  
1076 2024.
- 1077 Lüdecke, D., Ben-Shachar, M., Patil, I., Waggoner, P., & Makowski, D.: Performance: An R Package  
1078 for Assessment, Comparison and Testing of Statistical Models, *Journal of Open-Source Software*,  
1079 6(60), 3139, <https://doi.org/10.21105/joss.03139>, 2021.
- 1080 Luo, Y., & Zhou, X.: Methods of Measurements and Estimations. In Y. Luo & X. Zhou (eds) *Soil*  
1081 *Respiration and Environment*, 161-185 p., Academic Press, Elsevier,  
1082 <https://doi.org/10.1016/B978-0-12-088782-8.X5000-1>, 2006.
- 1083 Macharia, J. M., Pelster, D. E., Ngetich, F. K., Shisanya, C. A., Mucheru-Muna, M., & Mugendi, D. N.:  
1084 Soil greenhouse gas fluxes from maize production under different soil fertility management  
1085 practices in East Africa, *Journal of Geophysical Research: Biogeosciences*, 125(7),  
1086 e2019JG005427, <https://doi.org/10.1029/2019JG005427>, 2020.
- 1087 Malou, O. P., Moulin, P., Chevallier, T., Masse, D., Vayssières, J., Badiane-Ndour, N. Y., Tall, L., Thiam,  
1088 A., & Chapuis-Lardy, L.: Estimates of carbon stocks in sandy soils cultivated under local  
1089 management practices in Senegal's groundnut basin, *Regional Environmental Change*, 21(3), 65,  
1090 <https://doi.org/10.1007/s10113-021-01790-2>, 2021.



- 1091 Manzoni, S., Chakrawal, A., Fischer, T., Schimel, J. P., Porporato, A., & Vico, G.: Rainfall  
1092 intensification increases the contribution of rewetting pulses to soil heterotrophic respiration,  
1093 *Biogeosciences*, 17(15), 4007-4023, <https://doi.org/10.5194/bg-17-4007-2020>, 2020.
- 1094 Mapanda, F., Mupini, J., Wuta, M., Nyamangara, J., & Rees, R. M.: A cross-ecosystem assessment of  
1095 the effects of land cover and land use on soil emission of selected greenhouse gases and related  
1096 soil properties in Zimbabwe, *European Journal of Soil Science*, 61(5), 721-733,  
1097 <https://doi.org/10.1111/j.1365-2389.2010.01266.x>, 2010.
- 1098 Mazza, G., Agnelli, A. E., & Lagomarsino, A.: The effect of tree species composition on soil C and N  
1099 pools and greenhouse gas fluxes in a Mediterranean reforestation, *Journal of Soil Science and Plant*  
1100 *Nutrition*, 21(2), 1339-1352, <https://doi.org/10.1007/s42729-021-00444-w>, 2021.
- 1101 Mbow, C., Van Noordwijk, M., Luedeling, E., Neufeldt, H., Minang, P. A., & Kowero, G.: Agroforestry  
1102 solutions to address food security and climate change challenges in Africa, *Current Opinion in*  
1103 *Environmental Sustainability*, 6(1), 61-67, <https://doi.org/10.1016/j.cosust.2013.10.014>, 2014.
- 1104 Meena, A., Hanief, M., Dinakaran, J., & Rao, K. S.: Soil moisture controls the spatio-temporal pattern  
1105 of soil respiration under different land use systems in a semi-arid ecosystem of Delhi, India,  
1106 *Ecological Processes*, 9(1), 15, <https://doi.org/10.1186/s13717-020-0218-0>, 2020.
- 1107 Meisner, A., Rousk, J., & Bååth, E.: Prolonged drought changes the bacterial growth response to  
1108 rewetting, *Soil Biology and Biochemistry*, 88, 314-322,  
1109 <https://doi.org/10.1016/j.soilbio.2015.06.002>, 2015.
- 1110 Merbold, L., Ardo, J., Arneth, A., Scholes, R. J., Nouvellon, Y., de Grandcourt, A., Archibald, S.,  
1111 Bonnefond, J. M., Boulain, N., Brueggemann, N., Bruemmer, C., Cappelaere, B., Ceschia, E., El-Khidir,  
1112 H. A. M., El-Tahir, B. A., Falk, U., Lloyd, J., Kergoat, L., Le Dantec, V. L., Mougou, E., Muchinda, M.,  
1113 Mukelabai, M. M., Ramier, D., Rouspard, O., Timouk, F., Veenendaal, E. M., & Kutsch, W. L.:  
1114 Precipitation as driver of carbon fluxes in 11 African ecosystems, *Biogeosciences*, 6:1027-1041,  
1115 <https://doi.org/10.5194/bg-6-1027-2009>, 2009.
- 1116 Moncrieff, J., Clement, R., Finnigan, J., Meyers, T.: Averaging, Detrending, and Filtering of Eddy  
1117 Covariance Time Series. In: Lee, X., Massman, W., Law, B. (eds) *Handbook of Micrometeorology*,  
1118 *Atmos. Ocean. Sci. Lib.*, vol 29, Springer, Dordrecht, [https://doi.org/10.1007/1-4020-2265-4\\_2](https://doi.org/10.1007/1-4020-2265-4_2),  
1119 2004.
- 1120 Moncrieff, J. B., Massheder, J. M., De Bruin, H., Elbers, J., Friborg, T., Heusinkveld, B., Kabat, P., Scott,  
1121 S., Soegaard, H., Verhoef, A.: A system to measure surface fluxes of momentum, sensible heat, water



- 1122 vapour and carbon dioxide, *Journal of Hydrology*, 188, 589-611, [https://doi.org/10.1016/S0022-](https://doi.org/10.1016/S0022-1694(96)03194-0)  
1123 [1694\(96\)03194-0](https://doi.org/10.1016/S0022-1694(96)03194-0), 1997.
- 1124 Mosongo, P. S., Pelster, D. E., Li, X., Gaudel, G., Wang, Y., Chen, S., Li, W., Mburu, D., & Hu, C.:  
1125 Greenhouse Gas Emissions Response to Fertilizer Application and Soil Moisture in Dry  
1126 Agricultural Uplands of Central Kenya, *Atmosphere*, 13(3), 463,  
1127 <https://doi.org/10.3390/atmos13030463>, 2022.
- 1128 Muggeo, V.M.R.: Estimating regression models with unknown break-points. *Statist. Med.*, 22:  
1129 3055-3071, <https://doi.org/10.1002/sim.1545>, 2003.
- 1130 Munjonji, L., Ntuli Innocentia, H., Ayisi, K. K., Dlamini, P., Mabitsela, K. E., Lehutjo, C. M., &  
1131 Magnificent Zwane, P. S.: Seasonal dynamics of soil CO<sub>2</sub> emissions from different semi-arid land-  
1132 use systems, *Acta. Agr. Scand., Section BSP*, 74(1), 2312934,  
1133 <https://doi.org/10.1080/09064710.2024.2312934>, 2024.
- 1134 Nickerson, N. R.: Evaluating gas emission measurements using Minimum Detectable Flux (MDF),  
1135 Eosene White papers, [https://eosense.com/wp-content/uploads/2019/11/Eosense-white-](https://eosense.com/wp-content/uploads/2019/11/Eosense-white-paper-Minimum-Detectable-Flux.pdf)  
1136 [paper-Minimum-Detectable-Flux.pdf](https://eosense.com/wp-content/uploads/2019/11/Eosense-white-paper-Minimum-Detectable-Flux.pdf), 2016.
- 1137 Owusu-Prempeh, N., Amekudzi, L. K., & Kyereh, B.: Assessment of soil carbon dioxide efflux from  
1138 contrasting land uses in a semi-arid savannah ecosystem, northeastern Ghana (West Africa),  
1139 *Scientific African*, 26, e02420, <https://doi.org/10.1016/j.sciaf.2024.e02420>, 2024.
- 1140 Oyonarte, C., Rey, A., Raimundo, J., Miralles, I., & Escribano, P.: The use of soil respiration as an  
1141 ecological indicator in arid ecosystems of the SE of Spain: Spatial variability and controlling  
1142 factors, *Ecological Indicators*, 14(1), 40-49, <https://doi.org/10.1016/j.ecolind.2011.08.013>,  
1143 2012.
- 1144 Padfield, D., Matheso, G., & Windram, F.: Package 'Nls. Multstart : Robust Non-Linear Regression  
1145 using AIC Scores (R package version 2.0.0)', [DOI:10.32614/CRAN.package.nls.multstart](https://cran.r-project.org/web/packages/nls.multstart/nls.multstart.pdf),  
1146 <https://cran.r-project.org/web/packages/nls.multstart/nls.multstart.pdf>, 2025.
- 1147 Pelster, D., Rufino, M., Rosenstock, T., Mango, J., Saiz, G., Diaz-Pines, E., Baldi, G., & Butterbach-Bahl,  
1148 K., Smallholder farms in eastern African tropical highlands have low soil greenhouse gas fluxes,  
1149 *Biogeosciences*, 14(1), 187-202, <https://doi.org/10.5194/bg-14-187-2017>, 2017.



- 1150 Picarro Inc.: PICARRO G2508 CRDS Analyzer N<sub>2</sub>O + CH<sub>4</sub> + CO<sub>2</sub> + NH<sub>3</sub> + H<sub>2</sub>O in Air, [Datasheet],  
1151 [https://www.picarro.com/sites/default/files/product\\_documents/Picarro\\_G2508%20Analyzer](https://www.picarro.com/sites/default/files/product_documents/Picarro_G2508%20Analyzer%20Datasheet.pdf)  
1152 [%20Datasheet.pdf](https://www.picarro.com/sites/default/files/product_documents/Picarro_G2508%20Analyzer%20Datasheet.pdf), 2015.
- 1153 Placella, S. A., Brodie, E. L., & Firestone, M. K.: Rainfall-induced carbon dioxide pulses result from  
1154 sequential resuscitation of phylogenetically clustered microbial groups, Proceedings of the  
1155 National Academy of Sciences, 109(27), 10931-10936,  
1156 <https://doi.org/10.1073/pnas.1204306109>, 2012.
- 1157
- 1158 Pontauiller, J. Y., Hymus, G. J., & Drake, B. G.: Estimation of leaf area index using ground-based  
1159 remote sensed NDVI measurements: Validation and comparison with two indirect techniques,  
1160 Canadian Journal of Remote Sensing, 29(3), 381-387, <https://doi.org/10.5589/m03-009>, 2003.
- 1161 Poyda, A., Reinsch, T., Skinner, R. H., Kluß, C., Loges, R., & Taube, F.: Comparing chamber and eddy  
1162 covariance based net ecosystem CO<sub>2</sub> exchange of fen soils; Journal of Plant Nutrition and Soil  
1163 Science, 180(2), 252-266, <https://doi.org/10.1002/jipln.201600447>, 2017.
- 1164 Qiu, R., Han, G., Li, S., Tian, F., Ma, X., & Gong, W.: Soil moisture dominates the variation of gross  
1165 primary productivity during hot drought in drylands, Science of The Total Environment, 899,  
1166 165686, <https://doi.org/10.1016/j.scitotenv.2023.165686>, 2023.
- 1167 Quansah, E., Mauder, M., Balogun, A. A., Amekudzi, L. K., Hingerl, L., Bliefernicht, J., & Kunstmann,  
1168 H.: Carbon dioxide fluxes from contrasting ecosystems in the Sudanian Savanna in West Africa,  
1169 Carbon Balance and Management, 10(1), 1. <https://doi.org/10.1186/s13021-014-0011-4>, 2015.
- 1170 Rabbi, S. M. F., Warren, C., Swarbrick, B., Minasny, B., Mcbratney, A., & Young, I.: Microbial  
1171 decomposition of organic matter and wetting–drying promotes aggregation in artificial soil but  
1172 porosity increases only in wet-dry condition, Geoderma, 447, 116924,  
1173 <https://doi.org/10.1016/j.geoderma.2024.116924>, 2024.
- 1174 Rahimi, J., Ago, E. E., Ayantunde, A., Berger, S., Bogaert, J., Butterbach-Bahl, K., Cappelaere, B.,  
1175 Cohard, J.-M., Demarty, J., Diouf, A. A., Falk, U., Haas, E., Hiernaux, P., Kraus, D., Rouspard, O., Scheer,  
1176 C., Srivastava, A. K., Tagesson, T., & Grote, R.: Modeling gas exchange and biomass production in  
1177 West African Sahelian and Sudanian ecological zones, Geoscientific Model Development, 14(6),  
1178 3789-3812, <https://doi.org/10.5194/gmd-14-3789-2021>, 2021.



- 1179 Raich, J. W., Lambers, H., & Oliver, D. J.: Respiration in Terrestrial Ecosystems, In D. M. Karl, & W.  
1180 H., Schlesinger (Eds.), *Treatise on Geochemistry* (2 ed., Vol. 10, pp. 613-649), Elsevier,  
1181 <https://doi.org/10.1016/B978-0-08-095975-7.00817-2>, 2014.
- 1182 Ramesh, T., Manjaiah, K. M., Tomar, J. M. S., & Ngachan, S. V.: Effect of multipurpose tree species on  
1183 soil fertility and CO<sub>2</sub> efflux under hilly ecosystems of Northeast India, *Agr. Syst.*, 87(6), 1377-1388,  
1184 <https://doi.org/10.1007/s10457-013-9645-6>, 2013.
- 1185 R. Core Team.: R: A language and environment for statistical computing, R Foundation for  
1186 Statistical Computing, Vienna, Austria, 2023.
- 1187 Reichle, D. E.: Energy flow in ecosystems., In D.E. Reichle (ed) *The Global Carbon Cycle and Climate*  
1188 *Change* (p. 119-156), Elsevier, <https://doi.org/10.1016/B978-0-12-820244-9.00008-1>, (2020).
- 1189 Reichstein, M., Falge, E., Baldocchi, D., Papale, D., Aubinet, M., Berbigier, P., Bernhofer, C.,  
1190 Buchmann, N., Gilmanov, T., Granier, A., Grünwald, T., Havránková, K., Ilvesniemi, H., Janous, D.,  
1191 Knohl, A., Laurila, T., Lohila, A., Loustau, D., Matteucci, G., ... Valentini, R.: On the separation of net  
1192 ecosystem exchange into assimilation and ecosystem respiration: Review and improved  
1193 algorithm, *Glob. Change Biol.*, 11(9), 1424-1439, [https://doi.org/10.1111/j.1365-](https://doi.org/10.1111/j.1365-2486.2005.001002.x)  
1194 [2486.2005.001002.x](https://doi.org/10.1111/j.1365-2486.2005.001002.x), 2005.
- 1195 Reum, F., Gerbig, C., Lavric, J. V., Rella, C. W., & Göckede, M.: Correcting atmospheric CO<sub>2</sub> and CH<sub>4</sub>  
1196 mole fractions obtained with Picarro analyzers for sensitivity of cavity pressure to water vapor,  
1197 *Atmos. Meas. Tech.*, 12(2), 1013-1027, <https://doi.org/10.5194/amt-12-1013-2019>, 2005.
- 1198 Rheault, K., Riis Christiansen, J., & Steenberg Larsen, K.: The role of tree species and microbes for  
1199 the development of net greenhouse gas fluxes from soils after afforestation of agricultural lands,  
1200 EGU General Assembly 2024, Vienna, Austria, 14-19 April 2024, EGU24-9718,  
1201 <https://doi.org/10.5194/egusphere-egu24-9718>, 2024.
- 1202 Richardson, J., Chatterjee, A., & Darrel Jenerette, G.: Optimum temperatures for soil respiration  
1203 along a semi-arid elevation gradient in southern California, *Soil Biology and Biochemistry*, 46,  
1204 89-95, <https://doi.org/10.1016/j.soilbio.2011.11.008>, 2012.
- 1205 Riederer, M., Serafimovich, A., & Foken, T.: Net ecosystem CO<sub>2</sub> exchange measurements by the  
1206 closed chamber method and the eddy covariance technique and their dependence on atmospheric  
1207 conditions, *Atmos. Meas. Tech.*, 7(4), 1057-1064, <https://doi.org/10.5194/amt-7-1057-2014>,  
1208 2014.



- 1209 Roby, M. C., Scott, R. L., Biederman, J. A., Smith, W. K., & Moore, D. J. P.: Response of soil carbon  
1210 dioxide efflux to temporal repackaging of rainfall into fewer, larger events in a semiarid grassland,  
1211 *Frontiers in Environmental Science*, 10. <https://doi.org/10.3389/fenvs.2022.940943>, 2022.
- 1212 Rolo, V., Rivest, D., Maillard, É., & Moreno, G.: Agroforestry potential for adaptation to climate  
1213 change: A soil-based perspective, *Soil Use and Management*, 39(3), 1006-1032,  
1214 <https://doi.org/10.1111/sum.12932>, 2023.
- 1215 Rong, Y., Ma, L., Johnson, D., & Yuan, F.: Soil respiration patterns for four major land-use types of  
1216 the agro-pastoral region of northern China, *Agr. Ecosyst Environ.*, 213, 142-150,  
1217 <https://doi.org/10.1016/j.agee.2015.08.002>, 2015.
- 1218 Rosenstock, T. S., Mpanda, M., Pelster, D. E., Butterbach-Bahl, K., Rufino, M. C., Thiong'o, M., Mutuo,  
1219 P., Abwanda, S., Rioux, J., Kimaro, A. A., & Neufeldt, H.: Greenhouse gas fluxes from agricultural  
1220 soils of Kenya and Tanzania: GHG Fluxes From Agricultural Soils of East Africa, *Journal of*  
1221 *Geophysical Research: Biogeosciences*, 121(6), 1568-1580,  
1222 <https://doi.org/10.1002/2016JG003341>, 2016.
- 1223 Roupsard, O., Ferhi, A., Granier, A., Pallo, F., Depommier, D., Mallet, B., Joly, H. I., & Dreyer, E.:  
1224 Reverse Phenology and Dry-Season Water Uptake by *Faidherbia albida* (Del.) A. Chev. in an  
1225 Agroforestry Parkland of Sudanese West Africa, *Functional Ecology*, 13(4), 460-472,  
1226 <http://www.jstor.org/stable/2656552>, 1999.
- 1227 Roupsard, O., Audebert, A., Ndour, A. P., Clermont-Dauphin, C., Agbohessou, Y., Sanou, J., Koala, J.,  
1228 Faye, E., Sambakhe, D., Jourdan, C., le Maire, G., Tall, L., Sanogo, D., Seghier, J., Cournac, L., & Leroux,  
1229 L.: How far does the tree affect the crop in agroforestry? New spatial analysis methods in a  
1230 *Faidherbia parkland*, *Agr. Ecosyst. Environ.*, 296, 106928,  
1231 <https://doi.org/10.1016/j.agee.2020.106928>, 2020.
- 1232 Sarr, M.S., Diouf D., Roupsard O., Rocheteau A., Orange D., et al.: Estimation of seasonal water use  
1233 of *Faidherbia albida* (Delile) A.Chev. in a Sahelian agroforestry parkland, *Biotechnol. Agron. Soc.*  
1234 *Environ.*, 27(3), 196-204, <https://doi.org/10.25518/1780-4507.20512>, 2023.
- 1235 Schimel, J., Balsler, T. C., & Wallenstein, M.: Microbial stress-response physiology and its  
1236 implications for ecosystem function, *Ecology*, 88(6), 1386-1394, <https://doi.org/10.1890/06-0219>, 2007.



- 1238 Sida, T. S., Baudron, F., Kim, H., & Giller, K. E.: Climate-smart agroforestry: *Faidherbia albida* trees  
1239 buffer wheat against climatic extremes in the Central Rift Valley of Ethiopia, *Agr. Forest Meteorol.*,  
1240 248, 339-347, <https://doi.org/10.1016/j.agrformet.2017.10.013>, 2018.
- 1241 Siegwart, L., Bertrand, I., Roupsard, O., Duthoit, M., & Jourdan, C.: Root litter decomposition in a  
1242 sub-Saharan agroforestry parkland dominated by *Faidherbia albida*, *Journal of Arid*  
1243 *Environments*, 198, 104696, <https://doi.org/10.1016/j.jaridenv.2021.104696>, 2022.
- 1244 Siegwart, L., Bertrand, I., Roupsard, O., & Jourdan, C.: Contribution of tree and crop roots to soil  
1245 carbon stocks in a Sub-Saharan agroforestry parkland in Senegal, *Agr. Ecosyst. Environ.*, 352,  
1246 108524, <https://doi.org/10.1016/j.agee.2023.108524>, 2023.
- 1247 Sileshi, G. W.: The magnitude and spatial extent of influence of *Faidherbia albida* trees on soil  
1248 properties and primary productivity in drylands, *Journal of Arid Environments*, 132, 1-14,  
1249 <https://doi.org/10.1016/j.jaridenv.2016.03.002>, 2016.
- 1250 Sileshi, G. W., Teketay, D., Gebrekirstos, A., & Hadgu, K.: Sustainability of *Faidherbia albida*-Based  
1251 Agroforestry in Crop Production and Maintaining Soil Health., In J. C. Dagar, S. R. Gupta, & D.  
1252 Teketay (eds), *Agroforestry for Degraded Landscapes: Recent Advances and Emerging*  
1253 *Challenges—Vol. 2* (p. 349-369), Springer Singapore, [https://doi.org/10.1007/978-981-15-](https://doi.org/10.1007/978-981-15-6807-7_12)  
1254 [6807-7\\_12](https://doi.org/10.1007/978-981-15-6807-7_12), 2020.
- 1255 Singh, S., Mayes, M., Kivlin, S., & Jagadamma, S.: How the Birch Effect differs in mechanisms and  
1256 magnitudes due to soil texture, *Soil Biology and Biochemistry*, 179, 108973,  
1257 <https://doi.org/10.1016/j.soilbio.2023.108973>, 2023.
- 1258 Soudani, K., Hmimina, G., Delpierre, N., Pontailier, J. Y., Aubinet, M., Bonal, D., Caquet, B., de  
1259 Grandcourt, A., Burban, B., Flechard, C., Guyon, D., Granier, A., Gross, P., Heinesh, B., Longdoz, B.,  
1260 Loustau, D., Moureaux, C., Ourcival, J. M., Rambal, S., Saint André.L, Dufrene, E.: Ground-based  
1261 Network of NDVI measurements for tracking temporal dynamics of canopy structure and  
1262 vegetation phenology in different biomes, *Remote Sensing of Environment*, 123, 234-245,  
1263 <https://doi.org/10.1016/j.rse.2012.03.012>, 2012.
- 1264 Skinner, R. H., & Wagner-Riddle, C.: Micrometeorological Methods for Assessing Greenhouse Gas  
1265 Flux., In M. A. Liebig, A. J. Franzluebbers, & R. F. Follett (eds) *Managing Agricultural Greenhouse*  
1266 *Gases: Coordinated Agricultural Research through GRACEnet to Address our Changing Climate* (p.  
1267 367-383), Elsevier, <https://doi.org/10.1016/B978-0-12-386897-8.00021-8>, 2012.



- 1268 Stephen, E. A., Evans, K. D., & Akwasi, A. A.: Effects of *Faidherbia albida* on some important soil  
1269 fertility indicators on agroforestry parklands in the semi-arid zone of Ghana, *Afr. J. Agr. Res.*,  
1270 15(2), 256-268, <https://doi.org/10.5897/ajar2019.14617>, 2020.
- 1271 Stetter, C., & Sauer, J.: Tackling climate change: Agroforestry adoption in the face of regional  
1272 weather extremes, *Ecological Economics*, 224, 108266,  
1273 <https://doi.org/10.1016/j.ecolecon.2024.108266>, 2024.
- 1274 Stojanović, M., Jocher, G., Kowalska, N., Szatniewska, J., Zavadilová, I., Urban, O., Čáslavský, J.,  
1275 Horáček, P., Acosta, M., Pavelka, M., & Marshall, J. D.: Disaggregation of canopy photosynthesis  
1276 among tree species in a mixed broadleaf forest, *Tree Physiology*, 44(7), tpa064,  
1277 <https://doi.org/10.1093/treephys/tpae064>, 2024.
- 1278 Tagesson, T., Ardö, J., Guiro, I., Cropley, F., Mbow, C., Horion, S., Ehammer, A., Mougín, E., Delon, C.,  
1279 Galy-Lacaux, C., & Fensholt, R.: Very high CO<sub>2</sub> exchange fluxes at the peak of the rainy season in a  
1280 West African grazed semi-arid savanna ecosystem, *Geografisk Tidsskrift - Danish Journal of*  
1281 *Geography*, 116(a), 93-109, <https://doi.org/10.1080/00167223.2016.1178072>, 2016.
- 1282 Tagesson, T., Fensholt, R., Cappelaere, B., Mougín, E., Horion, S., Kergoat, L., Nieto, H., Mbow, C.,  
1283 Ehammer, A., Demarty, J., & Ardö, J.: Spatiotemporal variability in carbon exchange fluxes across  
1284 the Sahel, *Agr. Forest Meteorol.*, 226-227(b), 108-118,  
1285 <https://doi.org/10.1016/j.agrformet.2016.05.013>, 2016.
- 1286 Tagesson, T., Fensholt, R., Cropley, F., Guiro, I., Horion, S., Ehammer, A., & Ardö, J.: Dynamics in  
1287 carbon exchange fluxes for a grazed semi-arid savanna ecosystem in West Africa. *Agr. Ecosyst.*  
1288 *Environ.*, 205, 15-24, <https://doi.org/10.1016/j.agee.2015.02.017>, 2015.
- 1289 Tang, J., Bolstad, P. V., Desai, A. R., Martin, J. G., Cook, B. D., Davis, K. J., & Carey, E. V.: Ecosystem  
1290 respiration and its components in an old-growth forest in the Great Lakes region of the United  
1291 States, *Agr. Forest Meteorol.*, 148(2), 171-185, <https://doi.org/10.1016/j.agrformet.2007.08.008>,  
1292 2008.
- 1293 Tang, X., Carvalhais, N., Moura, C., Ahrens, B., Koirala, S., Fan, S., Guan, F., Zhang, W., Gao, S.,  
1294 Magliulo, V., Buysse, P., Liu, S., Chen, G., Yang, W., Yu, Z., Liang, J., Shi, L., Pu, S., & Reichstein, M.:  
1295 Global variability of carbon use efficiency in terrestrial ecosystems, *Biogeochemistry: Land*,  
1296 <https://doi.org/10.5194/bg-2019-37>, 2019.



- 1297 Tucker, C. L., & Reed, S. C.: Low soil moisture during hot periods drives apparent negative  
1298 temperature sensitivity of soil respiration in a dryland ecosystem: A multi-model comparison,  
1299 *Biogeochemistry*, 128(1-2), 155-169, <https://doi.org/10.1007/s10533-016-0200-1>, 2016.
- 1300 Unger, S., Máguas, C., Pereira, J. S., David, T. S., & Werner, C.: The influence of precipitation pulses  
1301 on soil respiration – Assessing the “Birch effect” by stable carbon isotopes, *Soil Biology and*  
1302 *Biochemistry*, 42(10), 1800-1810, <https://doi.org/10.1016/j.soilbio.2010.06.019>, 2010.
- 1303 Valujeva, K., Pilecka-Ulcugaceva, J., Skiste, O., Liepa, S., Lagzdins, A., & Grinfelde, I.: Soil tillage and  
1304 agricultural crops affect greenhouse gas emissions from Cambic Calcisol in a temperate climate,  
1305 *Acta. Agr. Scand. B-S-P.*, 72(1), 835-846, <https://doi.org/10.1080/09064710.2022.2097123>,  
1306 2022.
- 1307 Van Haren, J. L. M., De Oliveira, R. C., Restrepo-Coupe, N., Hutyra, L., De Camargo, P. B., Keller, M.,  
1308 & Saleska, S. R.: Do plant species influence soil CO<sub>2</sub> and N<sub>2</sub> O fluxes in a diverse tropical forest?  
1309 *Journal of Geophysical Research: Biogeosciences*, 115, G03010,  
1310 <https://doi.org/10.1029/2009JG001231>, 2010.
- 1311 Vargas, R., Enrique, S. C. P., Serrano-Ortiz, P., Yuste, J. C., Domingo, F., López-Ballesteros, A., &  
1312 Oyonarte, C.: Hot-moments of soil CO<sub>2</sub> efflux in a water-limited grassland, *Soil Systems*, 2(3), 1-18,  
1313 <https://doi.org/10.3390/soilsystems2030047>, 2018.
- 1314 Vickers, D., & Mahrt, L.: Quality Control and Flux Sampling Problems for Tower and Aircraft Data,  
1315 *Journal of Atmospheric and Oceanic Technology*, 14(3), 512-526,  
1316 [http://dx.doi.org/10.1175/1520-0426\(1997\)014%3C0512:QCAFSP%3E2.0.CO;2](http://dx.doi.org/10.1175/1520-0426(1997)014%3C0512:QCAFSP%3E2.0.CO;2), 1997.
- 1317 Wachiye, S., Merbold, L., Vesala, T., Rinne, J., Räsänen, M., Leitner, S., & Pellikka, P.: Soil greenhouse  
1318 gas emissions under different land-use types in savanna ecosystems of Kenya, *Biogeosciences*,  
1319 17(8), 2149-2167, <https://doi.org/10.5194/bg-17-2149-2020>, 2020.
- 1320 Wang, M., Guan, D.-X., Han, S.-J., & Wu, J.-L.: Comparison of eddy covariance and chamber-based  
1321 methods for measuring CO<sub>2</sub> flux in a temperate mixed forest, *Tree Physiology*, 30(1), 149-163,  
1322 <https://doi.org/10.1093/treephys/tpp098>, 2010.
- 1323 Wang, Z., Ji, L., Hou, X., & Schellenberg, M. P.: Soil Respiration in Semiarid Temperate Grasslands  
1324 under Various Land Management, *PLOS ONE*, 11(1), e0147987,  
1325 <https://doi.org/10.1371/journal.pone.0147987>, 2016.



- 1326 Waring E., Quinn M., McNamara A., Arino de la Rubia E., Zhu H., Ellis S.: skimr: Compact and  
1327 Flexible Summaries of Data, R package (version 2.1.5), <https://github.com/ropensci/skimr/>,  
1328 <https://docs.ropensci.org/skimr/> (website), 2024.
- 1329 Warren, C. R. Response of osmolytes in soil to drying and rewetting. *Soil Biology and Biochemistry*,  
1330 70, 22-32, <https://doi.org/10.1016/j.soilbio.2013.12.008>, 2014.
- 1331 Webb, E. K., Pearman, G. I., & Leuning, R., Correction of flux measurements for density effects due  
1332 to heat and water vapour transfer. *Q. J. R. Meteorol. Soc.*, 106, 85-100,  
1333 <https://doi.org/10.1002/qj.49710644707>, 1980.
- 1334 Wieckowski, A., Vestin, P., Ardö, J., Roupsard, O., Ndiaye, O., Diatta, O., Ba, S., Agbohessou, Y.,  
1335 Fensholt, R., Verbruggen, W., Gebremedhn, H. H., & Tagesson, T.: Eddy covariance measurements  
1336 reveal a decreased carbon sequestration strength 2010–2022 in an African semiarid savanna,  
1337 *Glob. Change Biol.*, 30(9), e17509. <https://doi.org/10.1111/gcb.17509>, 2024.
- 1338 Wiesner, S., Desai, A. R., Duff, A. J., Metzger, S., & Stoy, P. C.: Quantifying the natural climate solution  
1339 potential of agricultural systems by combining eddy covariance and remote sensing. *Journal of*  
1340 *Geophysical Research: Biogeosciences*, 127(9), e2022JG006895,  
1341 <https://doi.org/10.1029/2022JG006895>, 2022.
- 1342 Wild, J., Kopecký, M., Macek, M., Šanda, M., Jankovec, J., & Haase, T.: Climate at ecologically relevant  
1343 scales: A new temperature and soil moisture logger for long-term microclimate measurement,  
1344 *Agr. Forest Meteorol.*, 268, 40-47, <https://doi.org/10.1016/j.agrformet.2018.12.018>, 2019.
- 1345 Williams, C.A., Hanan, N.P., Neff, J.C. et al.: Africa and the global carbon cycle, *Carbon Balance*  
1346 *Manage*, 2, 3, <https://doi.org/10.1186/1750-0680-2-3>, 2007.
- 1347 Williams, C. A., Hanan, N., Scholes, R. J., & Kutsch, W.: Complexity in water and carbon dioxide  
1348 fluxes following rain pulses in an African savanna, *Oecologia*, 161(3), 469-480,  
1349 <https://doi.org/10.1007/s00442-009-1405-y>, 2009.
- 1350 Wohlfahrt, G., & Galvagno, M.: Revisiting the choice of the driving temperature for eddy covariance  
1351 CO<sub>2</sub> flux partitioning, *Agr. Forest Meteorol.*, 237-238, 135-142,  
1352 <https://doi.org/10.1016/j.agrformet.2017.02.012>, 2017.
- 1353 Wutzler, T., Lucas-Moffat, A., Migliavacca, M., Knauer, J., Sickel, K., Šigut, L., Menzer, O., and  
1354 Reichstein, M.: Basic and extensible post-processing of eddy covariance flux data with REdDyProc,  
1355 *Biogeosciences*, 15, 5015–5030, <https://doi.org/10.5194/bg-15-5015-2018>, 2018.



- 1356 Xenakis, G.: FREddyPro: Post-Processing EddyPro Full Output File. Edinburgh, UK. R package  
1357 version 1.0.1., 2016.
- 1358 Xue, H., & Tang, H.: Responses of soil respiration to soil management changes in an agropastoral  
1359 ecotone in Inner Mongolia, China, *Ecology and Evolution*, 8(1), 220-230,  
1360 <https://doi.org/10.1002/ece3.3659>, 2018.
- 1361 Yan, L., Chen, S., Xia, J., & Luo, Y.: Precipitation regime shift enhanced the rain pulse effect on soil  
1362 respiration in a semi-arid steppe, *PLoS ONE*, 9(8),  
1363 <https://doi.org/10.1371/journal.pone.0104217>, 2014.
- 1364 Yu, H., Xu, Z., Zhou, G., & Shi, Y.: Soil carbon release responses to long-term versus short-term  
1365 climatic warming in an arid ecosystem, *Biogeosciences*, 17(3), 781-792,  
1366 <https://doi.org/10.5194/bg-17-781-2020>, 2020.
- 1367 Yu, T., Jiapaer, G., Bao, A., Zheng, G., Zhang, J., Li, X., Yuan, Y., Huang, X., & Umuhoza, J.: Disentangling  
1368 the relative effects of soil moisture and vapor pressure deficit on photosynthesis in dryland  
1369 Central Asia, *Ecological Indicators*, 137, 108698, <https://doi.org/10.1016/j.ecolind.2022.108698>,  
1370 2022.
- 1371 Yu, X., Zha, T., Pang, Z., Wu, B., Wang, X., Chen, G., Li, C., Cao, J., Jia, G., Li, X., & Wu, H.: Response of  
1372 soil respiration to soil temperature and moisture in a 50-year-old oriental arborvitae plantation  
1373 in China, *PLoS ONE*, 6(12), <https://doi.org/10.1371/journal.pone.0028397>, 2011.
- 1374 Zaman M., Kleinedam K., Bakken L., Berendt J., Bracken C., Butterbach-Bahl K., Cai Z., Chang S. X.,  
1375 Clough T., Dawar K., Ding W. X., Dörsch P., dos Reis Martins M., Eckhardt C., Fiedler S., Frosch T.,  
1376 Goopy J., Görres C.-M., Gupta A., Henjes S., Hofmann M. E. G., Horn M. A., Jahangir M. M. R., Jansen-  
1377 Willems A., Lenhart K., Heng L., Lewicka-Szczebak D., Lucic G., Merbold L., Mohn J., Molstad L.,  
1378 Moser G., Murphy P., Sanz-Cobena A., Šimek M., Urquiaga S., Well R., Wrage-Mönnig N., Zaman S.,  
1379 Zhang J., Müller C.: Greenhouse Gases from Agriculture. In M. Zaman, L. Hang, C. Müller (eds)  
1380 Measuring emission of agricultural greenhouse gases and developing mitigation options using  
1381 nuclear and related techniques Springer, Cham, [https://doi.org/10.1007/978-3-030-55396-8\\_1](https://doi.org/10.1007/978-3-030-55396-8_1),  
1382 2021.
- 1383 Zeileis, A., Grothendieck, G., Ryan, J. A., Ulrich, J. M., & Andrews, F.: Package 'zoo': S3 Infrastructure  
1384 for Regular and Irregular Time Series (Z's Ordered Observations) (version 1.8-12) [R Package],  
1385 <https://zoo.R-Forge.R-project.org/>, 2024.



- 1386 Zhang, X., Bi, J., Zhu, D., & Meng, Z.: Seasonal variation of net ecosystem carbon exchange and gross  
1387 primary production over a Loess Plateau semi-arid grassland of northwest China, Scientific  
1388 Reports, 14(1), 2916, <https://doi.org/10.1038/s41598-024-52559-6>, 2024.
- 1389 Zhang, X., Ramakanth, K. K., & Long, Y.: The biomechanics of turgor pressure, Current Biology,  
1390 34(20), R986-R991, <https://doi.org/10.1016/j.cub.2024.07.013>, 2024.
- 1391 Zhao, C., Miao, Y., Yu, C., Zhu, L., Wang, F., Jiang, L., Hui, D., & Wan, S.: Soil microbial community  
1392 composition and respiration along an experimental precipitation gradient in a semiarid steppe,  
1393 Scientific Reports, 6(1), 24317, <https://doi.org/10.1038/srep24317>, 2016.
- 1394 Zhou, Y., Williams, C. A., Lauvaux, T., Feng, S., Baker, I. T., Wei, Y., Denning, A. S., Keller, K., & Davis,  
1395 K. J.: ACT-America: Gridded Ensembles of Surface Biogenic Carbon Fluxes, 2003-2019 (Version  
1396 1.1), ORNL Distributed Active Archive Center, <https://doi.org/10.3334/ORNLDAAC/1675>, 2019.
- 1397 Zhou, Y., Williams, C. A., Lauvaux, T., Davis, K. J., Feng, S., Baker, I., et al.: A multiyear gridded data  
1398 ensemble of surface biogenic carbon fluxes for North America: Evaluation and analysis of results,  
1399 Journal of Geophysical Research: Biogeosciences, 125, e2019JG005314,  
1400 <https://doi.org/10.1029/2019JG005314>, 2020.